COMPARATIVE STUDY ON THE FLEXURAL BEHAVIOUR OF GFRP REINFORCED CONCRETE BEAMS AND STEEL REINFORCED CONCRETE BEAMS

A Thesis Submitted in Fulfilment of the Requirement for the Award of the Degree of

MASTERS OF ENGINEERING

IN

STRUCTURAL ENGINEERING

Submitted by:

AMOL SINGH RAMANA

801724004

Under the supervision of

GURBIR KAUR
Assistant Professor, CED

RAJU SHARMA
Lecturer, CED

CIVIL ENGINEERING DEPARTMENT

THAPAR INSTITUTE OF ENGINEERING AND TECHNOLOGY

(Established under section 3 of UGC Act, 1956)

PATIALA-147004 (PUNJAB)

JULY 2019

DECLARATION

I, Amol Singh Ramana hereby declare that the work which is presented in this thesis entitled **"Comparative Study on the Flexural Behaviour of GFRP Reinforced Concrete Beams and Steel Reinforced Concrete Beams"** as per the requirements for the award of **Master of Engineering in Structures,** submitted in the **Civil Engineering Department, Thapar Institute of Engineering and Technology, Patiala,** is an authentic record of work carried out under supervision of **Dr. Gurbir Kaur, Assistant Professor, Department of Civil Engineering and Raju Sharma, Lecturer, Department of Civil Engineering, Thapar Institute of Engineering and Technology, Patiala** from January to July, 2019.

The matter presented herein has not been submitted either in part or full to any other university or institute for the award of any other degree.

Amol

Date: 5-09-2019 **(Amol Singh Ramana)**

This is to certify that the above declaration made by the student concerned is correct according to the best of my knowledge and belief.

(Raju Sharma)

Superviser

Lecturer, CED

T.I.E.T.

(Dr. Gurbir Kaur)

Superviser

Assistant Professor, CED

T.I.E.T

ACKNOWLEDGEMENT

I wish to offer my profound thanks **to Dr Gurbir Kaur, Assistant Professor Department of Civil Engineering** and **Raju Sharma, Lecturer, Department of Civil Engineering, Thapar Institute of Engineering and Technology, Patiala,** for giving their uncanny direction, support and for his patient tuning in of my thoughts and furthermore recommending new ways for actualizing my thoughts and for the inspiration and motivation and activated me all through my work. I might likewise want to thank every one of the resources and staff individuals for giving all the assistance and facilities, which I required for the completion of the thesis.

Amol

(Amol Singh Ramana)

801724004

ABSTRACT

Production of steel is a lengthy process which takes a lot of capital and effort to make it possible also the production of steel is also causing the generation of lots of pollutants and waste products. Steel production cannot be possible at the small units. So, it is not possible to establish production units of steel at small distances which increase the transportation costs also large projects like steel production are out of reach to the small investors which just produce wealth for already large investors. Presently multi day's manageable infrastructural development requests the elective material that ought to fulfil specialized necessities of basic steel, just as some different properties which steel doesn't convey, ought to be available. As a result, Glass fibres are mixed with resins (adhesives) to make a stiff bar type element known as GFRP bars are produced.

This thesis presents to take a shot at the reasonableness of GFRP bars as an option in contrast to traditional steel i.e. HYSD bars. This present work shows of properties such as flexural strength (at the ultimate moment and cracking moment), deflection-load properties, ductility, energy absorption and crack pattern analysis of GFRP-steel beams and conventional steel beams. The presented work would prove to be very useful in understanding the behaviour of beams made by replacing conventional steel bars by GFRP. Use of GFRP bars in creating beams provides a satisfactory solution to some of the main problem of corrosion and environmental problems associated with steel industries. Four arrangements of steel-RC beams and GFRP-RC beam are compared with each other after designing each arrangement for the same ultimate moment in both steel-RC and GFRP-RC beam. The test results mostly depend on the reinforcement ratio in both the beams. However, steel beams have shown good results in comparison but if results are compromised by other factors like cost, corrosion resistance, light-weightiness and some other factor than GFRP bars can be replaced by steel. New formulas are also prepared of ultimate moment capacity in the thesis which gives good agreement with experimental values.

LIST OF CONTENTS

DECLARATION.....I

ACKNOWLEDGMENT.....II

ABSTRACT.....III

LIST OF CONTENTS.....IV

LIST OF TABLES.....VII

LIST OF FIGURES.....IX

CHAPTER 1 INTRODUCTION

1.1. GENERAL.....1
1.2. TYPES OF FRPs (FIBRE REINFORCED POLYMER).....2
1.3. TYPES OF GLASS FIBRES (USED IN GFRP) AND THEIR PROPERTIES.....2
1.4. TYPES OF RESINS (USED IN GFRP) AND THEIR PROPERTIES.....3
1.5. PROCESS FOR MANUFACTURING GFRP (PULTRUSION).....4
1.6. PROPERTIES OF GFRP FIBRES AND BARS.....6

CHAPTER 2 LITERATURE REVIEW

2.1. GENERAL.....9
2.2. BOND PERFORMANCE OF GFRP BARS AND CONCRETE.....9
2.3. FLEXURE STRENGTH TESTING OF GFRP BEAMS.....12
2.3.1. Check for Ultimate load carrying capacity and load-carrying capacity without cracks.....13
2.3.2. Deflection.....18
2.3.3. Ductility.....22
2.4. OBSERVATIONS AND GAPS KNOWN FROM THE LITERATURE REVIEW.....23
2.5. OBJECTIVES OF THE PRESENT WORK.....24

CHAPTER 3 EXPERIMENTAL METHODOLOGY

3.1. GENERAL.....25
3.2. MATERIALS.....25
3.2.1. Ordinary Portland Cement (OPC 43).....25
3.2.2. Coarse Aggregate.....25
3.2.3. Fine Aggregate.....26
3.2.4. Steel Rebars.....27
3.2.5. GFRP Rebars.....28
3.3. MIX DESGN.....29
3.4. CASTING PROCEDURE FOR BEAMS.....31
3.4.1. Configuration of Steel bars and GFRP bars in Beams.....32
3.4.2. Casting of Beams.....34
3.4.3. Curing Procedure of Beams.....36
3.5. EXPERIMENTAL SETUP FOR TESTING BEAMS.....37

CHAPTER 4 RESULTS AND DISCUSSION

4.1. GENERAL.....39
4.2. ULTIMATE MOMENT CAPACITY OF BEAMS.....39
4.2.1. Calculated and Experimental Values of Ultimate Forces and Moments of Steel Beams.....39
4.2.2. Calculated and Experimental Values of Ultimate Forces and Moments of GFRP-Steel Beams.....41
4.2.3. Comparison between Control Beams and GFRP-Steel Beams on Ultimate Load-Carrying Capacity.....42
4.3. MID-SPAN DEFLECTION IN BEAMS UNDER TWO-POINT LOAD TEST.....43
4.3.1. Calculated and Experimental Values of Mid-Span Deflection of Steel Beams...44
4.3.2. Calculated and Experimental Values of Mid-Span Deflection of GFRP-Steel Beams.....45
4.3.3. Comparison between Steel Beams and GFRP-Steel Beams on End Deflection...45
4.4. LOAD-DEFLECTION BEHAVIOURS.....46
4.4.1. Load-Deflection of Behaviours of Steel Beams.....46
4.4.2. Load-Deflection of Behaviours of GFRP-Steel Beams.....47
4.4.3. Comparison between Steel Beams and GFRP-Beams on Load –Deflection Behaviour.....47
4.5. DUCTILITY OF BEAMS.....50
4.5.1. Ductility Factor Calculation of Steel Beams.....50
4.5.2. Ductility Factor Calculation of GFRP-Steel Beams.....51
4.5.3. Comparison of Ductility of Steel Beams and GFRP-Steel Beams.....51
4.6. ENERGY ABSORPTION OF BEAMS.....52
4.6.1. Energy Absorption of Steel Beams.....52
4.6.2. Energy Absorption of GFRP-Steel Beams.....53
4.6.3. Comparison of Energy Absorption of the Steel Beams and GFRP-Steel Beams.....53
4.7. CRACK PATTERN ANALYSIS OF BEAMS.....54
4.7.1. Crack Patterns of Control Beams.....54
4.7.1.1. Crack Patterns of S1 Beams.....54
4.7.1.2. Crack Patterns of S2 Beams.....56
4.7.1.3. Crack Patterns of S3 Beams.....58
4.7.1.4. Crack Patterns of S4 Beams.....60
4.7.2. Crack Patterns of Control Beams.....62
4.7.2.1. Crack Patterns of G1 Beams.....62
4.7.2.2. Crack Patterns of G2 Beams.....64
4.7.2.3. Crack Patterns of G3 Beams.....66
4.7.2.4. Crack Patterns of G4 Beams.....68
4.7.3. Comparison of Crack Patterns of Control and GFRP-Steel Beams.....68

CHAPTER 5 CONCLUSION

5.1. GENERAL.....70
5.2. FUTURE SCOPE OF WORK.....71

ANNEXURE-A.....72

ANNEXURE-B.....74

ANNEXURE-C.....78

ANNEXURE-D.....80

REFRENCES.....82

LIST OF TABLES

Table no.	Table topic	Page Number
1.1.	Mechanical and physical properties of glass fibres	3
1.2.	Some mechanical and physical properties of Polyester, Epoxy and Vinyl ester resins	4
1.3.	Mechanical characteristics of distinct diameters of GFRP bars	8
2.1.	Characteristic of GFRP beams	13
2.2.	Result of the flexure strength test	14
2.3.	Results of tensile strength, bending measurement	15
2.4.	Results of compressive strength of concrete	15
2.5.	Flexure strength result after 7 and 28 days of different type reinforced beam	15
2.6.	Tensile test result of GFRP bars	16
2.7.	Properties of concrete	16
2.8.	Three-point flexure test results	16
2.9.	Mechanical properties of GFRP bars	17
2.10.	Characteristics of beams	17
2.11.	Test result of various parameters	18
2.12.	Result of the ultimate strains both at bottom and top of beams	18
2.13.	Showing deflection at 50% ultimate moment	21
2.14.	Deflection at service load	22
2.15.	Deflection at 1.3 times service load	22
2.16.	Deformability factors of beams	23
3.1.	Properties showing physical behaviour of cement	25
3.2.	Coarse aggregate physical properties (60% of largest size 20mm and 40% of largest size 10mm)	26
3.3.	Coarse aggregate fineness modulus (60% of largest size 20mm and 40% of largest size 10mm)	26
3.4.	Fine aggregate physical properties	26
3.5.	Fine aggregate fineness modulus	27
3.6.	Strengthening properties of Fe500 steel (IS-1786:2008)	27
3.7.	Strength in tension of different diameter GFRP bars	28
3.8.	Comparison of weight of steel and GFRP rebars	28
3.9.	Mix design for M30 and M35	29

3.10. First trial test of 7days cubes in CTM.....29
3.11. Second test trial of 7days cubes in CTM.....30
3.12. Test trial of 28days cubes in CTM.....31
3.13. Testing results of 28 days cubes in CTM.....31
3.14. Different reinforcement configuration of series-2 beams.....32
3.15. Different reinforcement configuration of series-1 beams.....33
4.1. Calculated ultimate forces and moments of M30 and M35 steel beams 40
4.2. Experimental ultimate forces and moments of M30 and M35 steel beams.....40
4.3. % error between calculated and experimental values of ultimate force of M30 and M35 steel beams.....40
4.4. Calculated ultimate forces and moments of M30 and M35 GFRP-Steel beams.....41
4.5. Experimental ultimate forces and moments of M30 and M35 GFRP-Steel beams.....41
4.6. % error between experimental and calculated values of ultimate force of M30 and M35 GFRP-Steel beams.....42
4.7. Percentage error in moment values when calculated of M30 and M35 beams when compared with each other.....42
4.8. Error in moment values when experimentally observed of M30 and M35 beams when compared with each other.....43
4.9. Difference in the calculated and experimental errors in the M30 and M35 beams.....43
4.10. Mid-span deflection comparisons calculated versus experimental of M30 and M35 steel beams.....44
4.11. Deflection comparison calculated versus experimental of M30 and M30 GFRP-Steel beams.....45
4.12. Comparison of averaged experimental deflection between M30beams.....45
4.13. Comparison of averaged experimental deflection between M35 beams.....46
4.14. Values of first crack and ductility factor of steel beams.....51
4.15. Values of first crack and ductility factor of GFRP-Steel beams.....51
4.16. Comparison between ductility factor of steel beams and GFRP-Steel beams.....52
4.17. Values of energy absorption of steel beams.....52
4.18. Values of energy absorption of steel beams.....53
4.19. Comparison between energy absorption of steel beams and GFRP-Steel beams.....53

LIST OF FIGURES

Figure no.	Figure topic	Page Number
1.1.	Fibreglass reinforcement production line	4
1.2.	Upgraded reinforcement roving unit of fibreglass	5
1.3.	The stress-strain behaviour in tension of multiple fibres	6
1.4.	Tensile stress-strain graph of three different GFPR bars made by different manufacturers and also of conventional steel used in Poland	7
1.5.	Graph showing decrement of shear strength and tensile strength with increase in diameter	9
2.1.	Force transfer mechanism between bar and concrete	10
2.2.	Stress-slip relationship of bond for GFRP bars with a different surface	11
2.3.	Schematic diagram illustrating impact on the FRP bond strength of environment	11
2.4.	Schematic diagram illustrating the bond strength impact of high temperature	12
2.5.	Load-deflection curve (a) GFRP beams and (b) comparison steel beam	21
3.1.	Weight oven dried fine sand	27
3.2.	GFRP bars of different diameters	28
3.3.	Cube samples in moulds	30
3.4.	Compressive strength testing of cube	30
3.5.	Sketch showing reinforcement placement of S1 and G1 beam	33
3.6.	Sketch showing reinforcement placement of S2 and G2 beam	33
3.7.	Sketch showing reinforcement placement of S3 and G3 beam	34
3.8.	Sketch showing reinforcement placement of S1 and G1 beam	34
3.9.	Steel and GFRP arrangements of beams	35
3.10.	Oiled moulds with Steel and GFRP arrangements of beams	35
3.11.	Beam specimens after dismantling	36
3.12.	Prepared beams were placed in plastic tanks for 28 days curing	36
3.13.	Experimental setup for testing beam in two-point loading test	37
3.14.	Bending moment and Shear force under two-point load arrangement	38
4.1.	Graphs of the all steel beams of both grade M30 and M35	46
4.2.	Graphs of the all GFRP-Steel beams of both grade M30 and M35	47
4.3.	Load-deflection curve of S1 and G1 beam of grade M30 and M35	48
4.4.	Load-deflection curve of S2 and G2 beam of grade M30 and M35	48
4.5.	Load-deflection curve of S3 and G3 beam of grade M30 and M35	49
4.6.	Load-deflection curve of S4 and G4 beam of grade M30 and M35	49
4.7.	Cracks in S1 (1) of grade M30 beam at ultimate load 46.95kN	54
4.8.	Cracks in S1 (1) of grade M30 beam at ultimate load 48.21kN	54

4.9. Cracks in S1 (1) of grade M35 beam at ultimate load 50.24kN.....55
4.10. Cracks in S1 (2) of grade M35 beam at ultimate load 52.16kN.....55
4.11. Cracks in S2 (1) of grade M30 beam at ultimate load 54.85kN.....56
4.12. Cracks in S2 (2) of grade M30 beam at ultimate load 72.34kN.....56
4.13. Cracks in S2 (1) of grade M35 beam at ultimate load 78.61kN.....57
4.14. Cracks in S2 (2) of grade M35 beam at ultimate load 58.03kN.....57
4.15. Cracks in S3 (1) of grade M30 beam at ultimate load 79.14kN.....58
4.16. Cracks in S3 (2) of grade M30 beam at ultimate load 80.8kN.....58
4.17. Cracks in S3 (1) of grade M35 beam at ultimate load 95.92kN.....59
4.18. Cracks in S3 (2) of grade M35 beam at ultimate load 84.15kN.....59
4.19. Cracks in S4 (1) of grade M30 beam at ultimate load 82.88kN.....60
4.20. Cracks in S4 (2) of grade M30 beam at ultimate load 85.11kN.....60
4.21. Cracks in S4 (1) of grade M35 beam at ultimate load 89.00kN.....61
4.22. Cracks in S4 (2) of grade M35 beam at ultimate load 98.63kN.....61
4.23. Cracks in G1 (1) of grade M30 beam at ultimate load 56.75kN.....62
4.24. Cracks in G1 (2) of grade M30 beam at ultimate load 52.7kN 62
4.25. Cracks in G1 (1) of grade M35 beam at ultimate load 53.67kN.....63
4.26. Cracks in G1 (2) of grade M35 beam at ultimate load 52.57kN.....63
4.27. Cracks in G2 (1) of grade M30 beam at ultimate load 67.75kN.....64
4.28. Cracks in G2 (2) of grade M30 beam at ultimate load 63.18kN.....64
4.29. Cracks in G2 (1) of grade M35 beam at ultimate load 49.92kN.....65
4.30. Cracks in G2 (2) of grade M35 beam at ultimate load 66.26kN.....65
4.31. Cracks in G3 (1) of grade M30 beam at ultimate load 68.23kN.....66
4.32. Cracks in G3 (2) of grade M30 beam at ultimate load 66.17kN.....66
4.33. Cracks in G3 (1) of grade M35 beam at ultimate load 89.91kN 67
4.34. Cracks in G3 (2) of grade M35 beam at ultimate load 56.93kN.....67
4.35. Cracks in G4 (1) of grade M30 beam at ultimate load 55.77kN.....68
4.36. Cracks in G4 (2) of grade M30 beam at ultimate load 80.2kN.....68
4.37. Cracks in G4 (1) of grade M35 beam at ultimate load 73.86kN.....69
4.38. Cracks in G4 (2) of grade M35 beam at ultimate load 90.7kN.....69
A1 New stress and strain diagram developed after removing partial safety factor.....72

CHAPTER-1

INTRODUCTION

1.1. GENERAL

From nearly 100 years the steel as a reinforcing agent in concrete because of the best results obtained from this combination in terms of strength and economical aspects. A lot of progress is made by updating the quality of steel and concrete by which we increased the strength of the structures by many folds. Major drawbacks of these materials that vast industry setups are needed to manufacture them (concrete and steel), by which a lot of capital is needed to invest initially. Lots of capital investment cause high construction costs by which it is impossible to construct at low costs. Even great problems that are faced by steel is that it is not perfectly recoverable after use and a lot of processes are needed to recover it and also afterwards recovery is not 100%. So, someday in future, the scarcity of steel will arrive and construction using steel will become expensive. Another problem with steel is its corrosive nature, if steel comes in contact with water and air, the corrosion takes place consequently, very disastrous to the lifespan of the structure. To prevent the structure from the corrosion, engineers are adopting various corrosion resistance techniques e.g. cathode-anode method, coating of steel with red oxide and other methods which further increase the cost of the project. So to cope up with these situations some other alternative is needed.

Recently the substitution of steel bars with fibre reinforced plastics (FRPs) bars to gain huge popularities in research. FRPs have same average lifespan of 100 years as steel, quite lighter than steel, does not possess magnetic property so does not show any change when it comes in contact with magnetic fields, it is also reported that the FRP bars have more tensile strength than the steel and most important that it does not show any change when they come in contact with the moisture. Nowadays many researchers are working on the FRP material in construction to improve the overall strength. Still, much work is needed to do on FRP like at what ratio it will be used get a particular amount of strength, no clear Indian standard formulas are made yet for FRP bars, by which it cannot be extensively used at construction sites. So for the derivation of the formulas compatibility of the FRP bars with concrete is needed to be defined i.e. bond strength or adhesion is present between FRP bars and concrete. Afterwards, the process of finding the strength of the different elements like beam, column, strut etc made by FRP and concrete should be continued. To know the compatibility of the FRP in construction such element should be used for testing which directly can relate to properties of FRP. So for this beam is a suitable element to start testing with because as

known from the earlier studies that in beam most of the tension is held by the steel reinforcement and most of the compressive forces are handled by the concrete. Likewise, the replacement of steel reinforcement can be done in the beams to know its tensile properties.

1.2. TYPES OF FRPs (FIBRE REINFORCED POLYMERS)

The major types of FRPs known are three in number which are mentioned below:-

1. GFRP (Glass fibre reinforced polymer) is made up of glass fibres which are made by melting glass and turning it to shape of fibres and resins. Further, all the thesis is based on GFRP so its manufacturing and its properties are discussed in the below sections.

2. CFRP (Carbon fibre reinforced polymer) is produced of a substance called precursor. 90 % of them are made up of polyacrylonitrile and 10% is produced up of rayon or petroleum pitch. Have high strength and used in many fields (medical, nano-tech, etc.).

3. AFRP (Aramid fibre reinforced polymer) is made up from fibres aramid also called as aromide polyamide and resins (binding material).

1.3.TYPES OF GLASS FIBRES (USED IN GFRP) AND THEIR PROPERTIES

As known from GFRP manufacturers, material GFRP is available in many forms but two types of it are used in prominent forms that are sheets and bars. Manufacturing process of bars is discussed below, GFRP is a mixed substance made up of glass fibre and an adhesive resin matrix. Glass fibre are made by extending the molten glass and making too thin in which it just comes to dimension of the small threads few chemicals are also mixed in the molten glass to bring flexibility to it. Likewise to make GFRP bar many of glass fibre filaments are put together longitudinally and between them, some kind of resins (adhesives) is applied which connect all filament firmly and give them affirm structure which can be utilized as reinforcement .

According to Benmokrane et al (1995), GFRP bars can be divided into four categories:-

1. E-glass
2. S-glass
3. AR-glass
4. C-glass

E-glass is lowest in cost perspective and in the properties like strength, stiffness and ultimate strain it is also lesser than S-glass. S-glass is much more attacked by the alkali environment.

Where AR-glass (alkali-resistant glass) is good in the alkali environment and C-glass is resistant to the acidic environment. The physical and mechanical properties of the above GFRPs are discussed in Table-1.1 given by Benmokrane et al (1995).

Table-1.1 Mechanical and physical properties of glass fibres (Benmokrane et al. 1995)

Parameter	AR-glass	C-glass	E-glass	S-glass
Tensile strength (GPa)	2.5	3.03	3.45	4.3
Tensile modulus (Gpa)	70.0	69.0	72.4	86.9
Ultimate strain (%)	3.6	4.8	4.8	5.0
Poisson's ratio	-	-	0.2	0.22
Density (g/cm^3)	2.78	2.49	2.54	2.49
Diameter (μm)	-	4.5	10.0	10.0
Longitudinal CTE ($10^{-6}/^oC$)	-	7.2	5.0	2.9
Dielectric constant	-	-	6.3	5.1

1.4.TYPES OF RESINS (USED IN GFRP) AND THEIR PROPERTIES

Now materials for the matrix which are mainly used in GFRP are

3.4.Polyester

3.5.Epoxy

3.6.Vinyl Ester

Polyester consists of unsaturated polymer ester mixed in a monomer like styrene cross-linking. The proportion of this can really vary its properties to a wide range. Polyesters are not degraded by fire, moisture, acids, and alkalis but have much bad effect when it comes in contact with chlorinated solvents. The most problematic features of polyester are its volumetric shrinkage during used in the manufacturing of GFRP.

Epoxy has elevated power and resistance to creep, powerful adhesion to solvent-resistant fibres and chemical resistance. It also has volatile emission and low shrinkage during curing. This epoxy resin also displays good electrical characteristics and a lot of glass transition temp erature.

A single functional unsaturated acid-like methacrylic or acrylic acid and epoxy resin produce vinyl ester resins. It has more chemical and high-temperature resistance than polyester. It also has a low viscosity which is suitable for manufacturing. High interfacial strength and better

wet-out are also present in the vinyl ester. Only major drawbacks are that it also has great volumetric shrinkage and also they are more costly than polyester.

Table-1.2 Some mechanical and physical properties of Epoxy, Polyester and Vinyl ester resins (Benmokrane et al. 1995)

Parameter	Polyester	Epoxy	Vinyl Ester
CTE (10^{-6}/°C)	55-100	45-90	21-73
Cure shrinkage (%)	5-12	1-5	5.4-10.3
Density (g/cm^3)	1.0-1.45	1.1-1.3	1.1-1.3
Poisson's ratio	-	0.2-0.33	-
Tensile modulus (Gpa)	2.1-4.1	2.5-4.1	3.0-3.5
Tensile strength (Mpa)	20-100	55-130	70-80
Ultimate strain (%)	1-6	1-9	3.5-5.5
T_g (°C)	100-140	50-260	90-140

1.5.PROCESS FOR MANUFACTURING GFRP (PULTRUSION)

The process which is used to combine the glass fibres and resins to make it GFRP bars is known as Pultrusion process. This process is explained by the help of Figure-1.1.

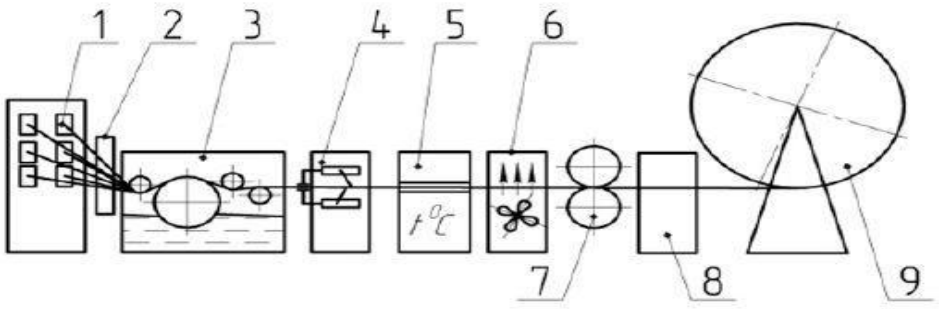

Figure-1.1 Fibreglass reinforcement production line (Maksimov et al. 2017)

The following are the processes which are numbered in Figure-1.1.

1. Pulling fibre filament of creel coil.
2. Initially heated up and dried.
3. Filaments are immersed with the adhesive in the paste pot, removing excess binder.
4. To form the ribbed surface and create the roving, impregnated strands are fed into the unit.
5. It is then passed to tunnel furnace for polymerization.
6. Intensive cooling is done with air or water-way.

7. Fibres on the pulling mechanism for promoting fibreglass strands and completing fittings at all manufacturing line phases.
8. It is a device which cuts GFRP to the specified length.
9. Storage is performed by winding to the bay or laying in the rack to the reinforcement rods.

According to Maksimov et al. (2017) that the above process is not much good to make GFRP because

1. It can affect the health of labour due to openly use of adhesive.
2. The adhesive is not used properly from the bottom of the tank which causes extension of the cleaning process and also wastage of adhesive.
3. Likewise, when glass fibre is dipped in the adhesive it takes much more than it needs to polymerize which also cause the same problem as above.
4. This all process cause low perfection in making of the GFRP bars which do not lead to healthy and fast production.

The new process is developed by Maksimov et al (2017) which is shown in Figure-1.2.

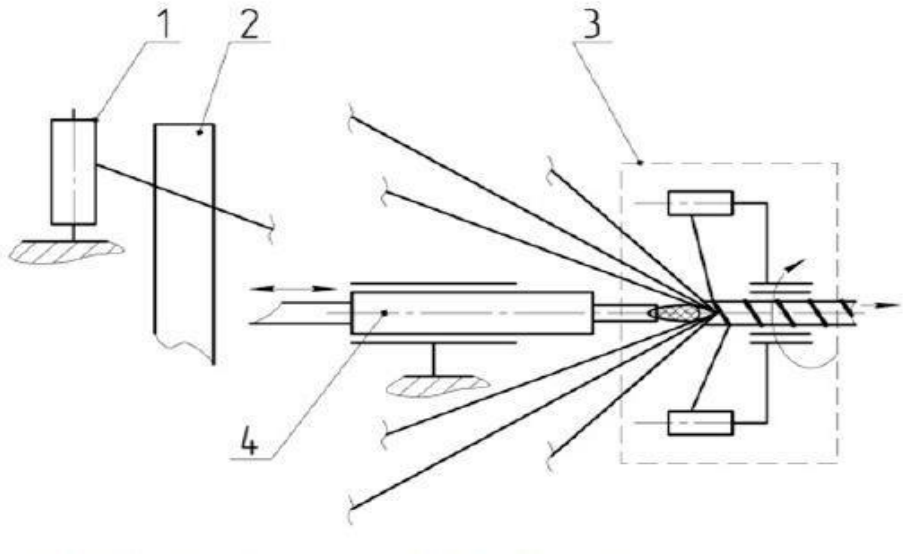

Figure-1.2 Upgraded reinforcement roving formation unit of fibreglass (Maksimov et al. 2017)

The following are the processes which are numbered in Figure-1.2.

1. Strands of fibreglass are supplied from the creel.
2. Fibreglasses are heated and dried.
3. This device is directly forming ribbed reinforcing surface.

4. The device has a nozzle which provides sufficient loads of adhesive to the fibreglass strands to make it GFRP.

All other later processes in Figure -1.2 are the same in this process shown in Figure-1.1. This is all about how GFRP bars are manufactured in the manufacturing unit. By seeing the whole process it can be concluded that it is quite simpler than the production of steel bars.

1.6.PROPERTIES OF GFRP FIBRES AND BARS

Much of the properties of materials predicted with help of the stress-strain graph of that property, so for the tensile property of the GFRP stress-strain graph is discussed below. Most of the properties of GFRP will depend on the glass because 60 % to 80% of GFRP is made of the glass and another percentage is conquered by resins (adhesives). So the property of the glass is known to be perfectly elastic till its breaking point. In American code, ACI 440R-96 different materials tensile stress-strain is given in Figure-1.3.

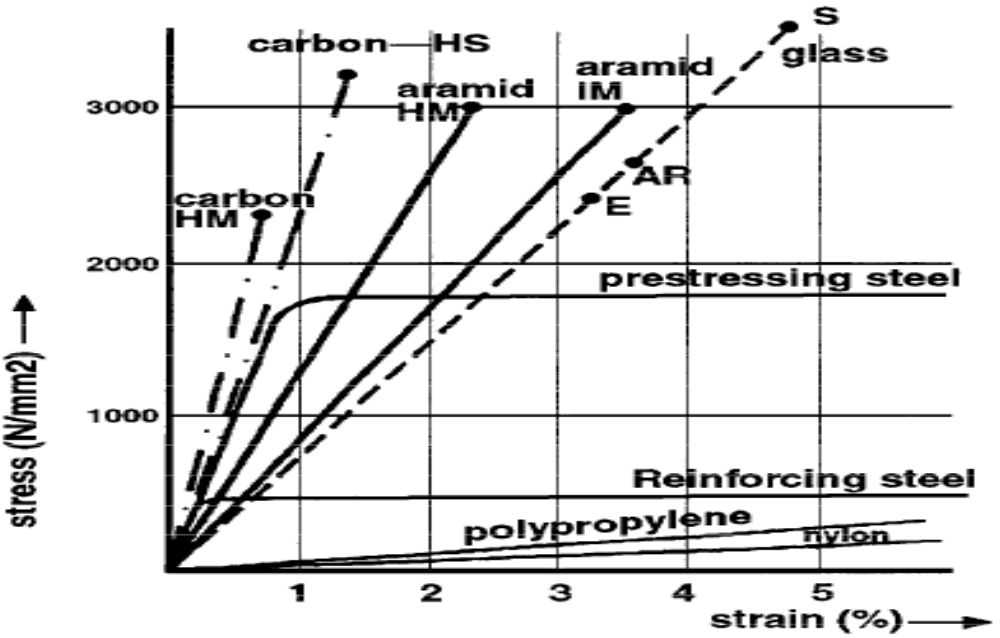

Figure-1.3 - The stress-stress behavior in tension of multiple fibers (Gerritse and Schurhoff 1993)

In Figure-1.3, it can be seen that utmost stress is taken by glass S-fibres and then AR and E-glass is quite good in the taking tensile stress which shows a good sign for the GFRP can be used in construction purposes. A stress-strain graph of GFRP is discussed by Jarek and Kubik (2015) in which they have taken rods of GRRP from three manufacturers (4 from first one, 4 from the second one, and 3 from the third one). They calculated the diameter of every bar and take it equivalent to 12mm with an error of -11% to 14%. After which they have tested all the

rods in the tensile testing machine up to the breakpoint. By doing the test they made an equivalent stress-strain graph of the entire GFRP manufacturer and compared it with conventional steel (AIIIN) graph (the graph is shown below). In this study, they find that Young's modulus of two types of bars which are manufactured by the different manufacturer shows the same value that is 54GPa whereas one of type Young's modulus near 39GPa. By this, conclusion can be drawn that Young's modulus of the GFRP bars vary manufacturer to manufacturer because no such hard guidelines are given in any code regarding quality maintenance during the construction of GFRP rebars.

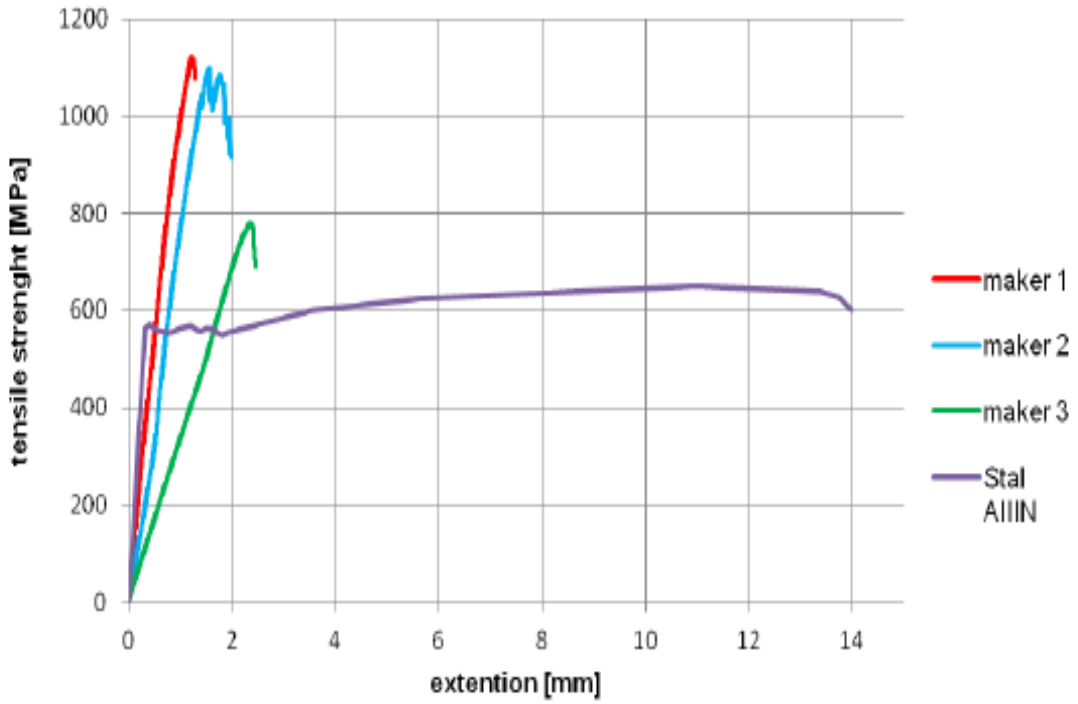

Figure-1.4 Tensile stress-strain graph of three different GFPR bars made by different manufacturers and also of conventional steel used in Poland (Jarek and Kubik 2015)

It can be concluded from Figure 1.4 that GFRP is a perfectly elastic material up to a certain point after which it starts breaking. Like steel, its elastic part in the graph can be used for making the structural elements; likewise, elastic part in the graph of the GFRP can also be used to make the structural elements. By all this process this is known that GFRP is an elastic material.

GFRP has also one of the major drawbacks that are of reduction in tensile strength by an increment of the diameter. Gu et al. (2016) have experimented on 18 different samples of the GFRP with a difference in the diameter and checked every piece for tensile strength and other properties and found the conclusion that is already discussed.

Table-1.3 Mechanical characteristics of distinct diameters of GFRP bars (Gu et al. 2016)

Diameter	3mm	4mm	6mm	8mm	10mm	12mm	14mm	16mm	18mm
Strength in tension (MPa)	2624	1988	1579	1218	1038	939	929	1016	896
Shear strength (MPa)	620	368	291	223	185	204	240	161	210
Elastic modulus (GPa)	41.2	41.4	41.6	41.5	41.4	41.5	41.3	41.2	41.2
Diameter	20mm	22mm	25mm	28mm	32mm	32mm	34mm	36mm	40mm
Strength in tension (MPa)	1005	917	1017	973	970	917	852	852	728
Shear strength (MPa)	188	191	187	181	161	157	161	159	157
Elastic modulus (GPa)	41.5	41.5	41.5	41.2	41.5	41.5	41.6	41.5	41.5

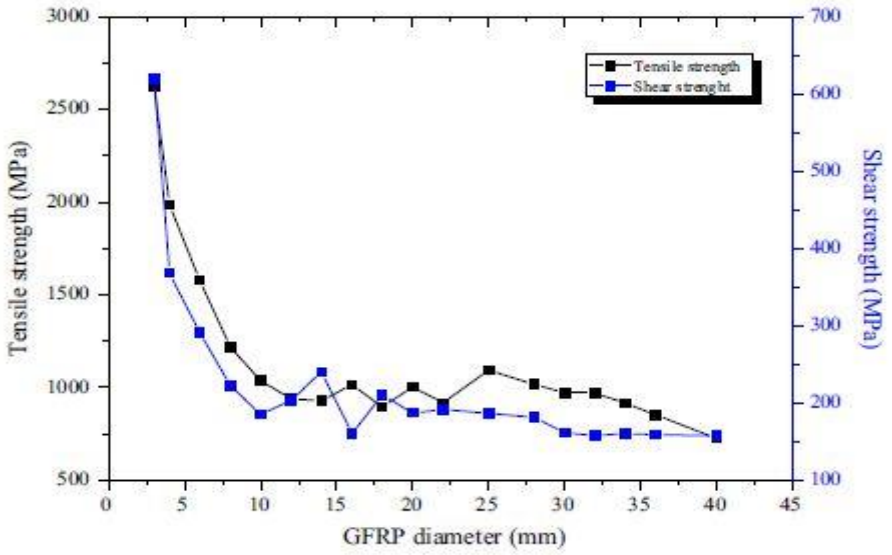

Figure -1.5 Graph showing decrement of shear strength and tensile strength with increase in diameter (Gu et al. 2016)

It can be concluded from Figure 1.5 that when the bigger diameter is used then the stress developed in the outer fibre is not transferred to the inner fibre as seen from the graph that after 10mm diameter tensile strength becomes nearly constant for all diameters.

CHAPTER-2

LITERATURE REVIEW

2.1. GENERAL

GFRP bars properties are known by above sections, to have a similarity of the elastic region in the stress-strain graph with steel so many of the researchers have shown interest in the GFRP bars and replace it with conventional steel from the structural elements and noticed many properties. Flexural properties of the beams which are fitted with GFRP bars have been noticed by many of the researchers and also been compared with the normal conventional steel beams, few of them are discussed in this section. Also, the bond properties of the GFRP and concrete were researched in details which are also disused in this section briefly.

2.2. BOND PERFORMANCE OF GFRP BARS AND CONCRETE

The main parameter arises between both material i.e. GFRP and concrete is bonding. If both materials do have good binding in between then we can use them extensively for the manufacturing of structures. According to Holly et al. (2016), the steel bars bonds depend on three components.

- Adhesion: the chemical bond between steel and concrete. It just plays a small role till the structure is not loaded when the structure is loaded then this type of bond vanishes.
- Mechanical interlocking: deformed bar shape causing mechanical interlocking with the concrete, so mostly steel rebar and concrete bonding relies on the ribs. Along with the steel rebar. When the ultimate strength of bond is reached then shear cracks begin to form on the surface.
- Friction: This is the characteristics of surface of concrete and bar, they form frictional bond between each other by which the bar slips out from the concrete.

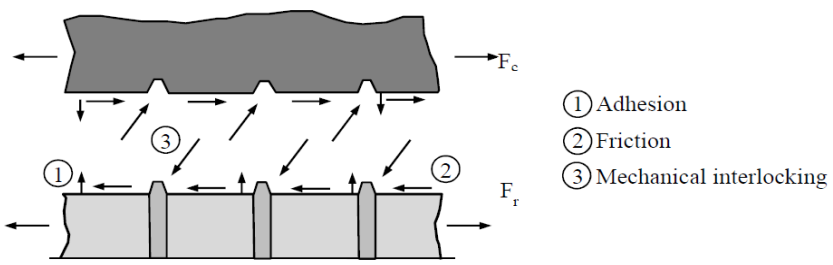

Figure-2.1 Force transfer mechanism between bar and concrete (Holly et al. 2016)

In GFRP and concrete, only two types of bonds are now that are friction and mechanical interlocking. Mechanical interlocking is present if GRFP bars are deformed otherwise only friction will be present if plain GFRP bars are used which will not be sufficient to make a bond between concrete and GFRP bar. Strength of bond of the GFRP is about 55% to 90% of the steel bars. Bond stresses of GFRP are given with different surface condition is shown in Figure – 2.1. According to Holly et al. (2016), the behaviour of bond of FRP bars straight or deformed relies on the following factors.

1. Confinement pressure: the bond of concrete and bar can only be sufficient if pressure of concrete near the bar is good which can only be possible if the concrete is provided with a good level of compaction with vibrators.
2. Bar diameter: as the diameter of bar increases surface area of bar also increases which give more space to concrete to make the bond with bar. So, as diameter of bar increases the strength of bond of the concrete and bar also increases.
3. Effect of position of bar in cast: if the concrete cover is less than twice the diameter of the bar then it is more likely that failure type will be splitting failure and if it is more than twice then pull out failure will dominate which take much more force than splitting failure.
4. Top-bar effect: When concrete is poured some lighter particles like air, water, and fine particles travel to the upper part of the poured concrete, these particles do not make a good bond with the bars causing the top-bar effect. Sometimes bond strength reduces to 66% than the bottom layer.
5. Embedment length: more the bar is embedded in concrete more the surface area will be contacted with concrete which will generate more bond strength between both bar and concrete.
6. Environment conditions: when GFRP bar is exposed to extreme climates it does not show good results due to regular contact with water, air and another factor which cause the rapid decrease in strength of bond and age reduction of the building. Strength of bond also decreases with time as the temperature changes also which is shown in Figure-2.3.
7. The condition of surface of bar: the conditions of surface of bar also play a great role in the bonding strength. Bars can surface conditions can be changed by making them ribbed, sand coated, braided and sanded etc. Bond stress in the different condition is displayed in Figure-2.2.

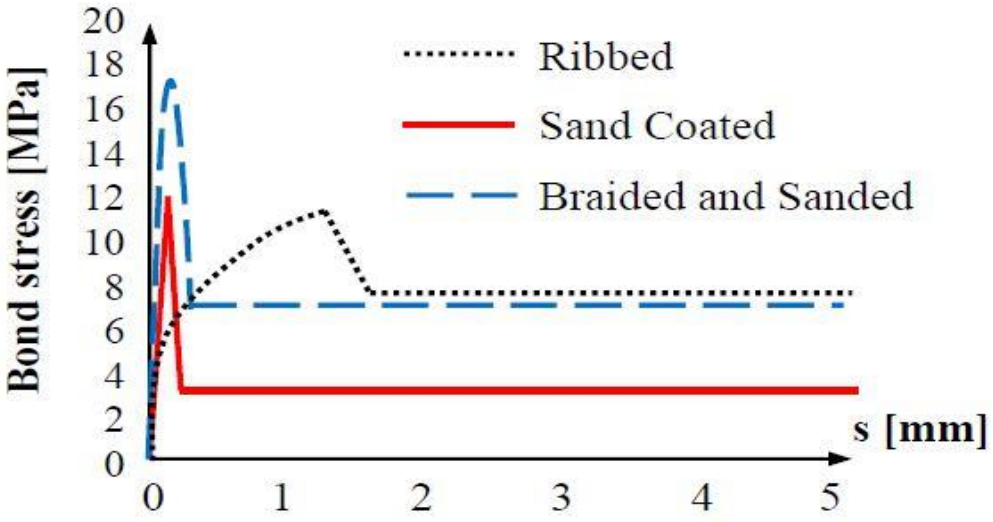

Figure-2.2 Stress-slip relationship of bond of GFRP bars with a different surface (Vint 2012)

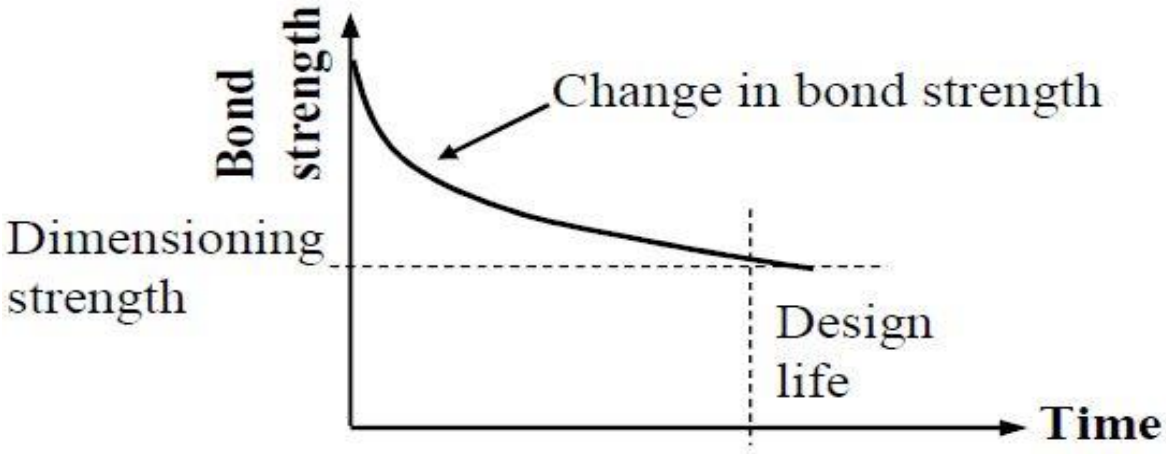

Figure- 2.3 Schematic diagram illustrating impact on the FRP bond strength of environment (Tepfers 2004)

8. Temperature change: GFRP bond with concrete also gets deteriorated when it comes in contact with the high temperature. GFRP bars begin to experience substantial thermal expansion resulting in demolished concrete cover and the growth of shear stress in their adhesive layer. GFRP can also catch fire causing emission of toxic gases. So GFRP must not be used at places where fire break down can happen. Even it is recommended that 30^0C higher temperature should be taken of the place as a design temperature, where GFRP is used and then GFRP bars should be selected according to the material. Figure-2.4 shows how bond strength decreases during the increase in temperature.

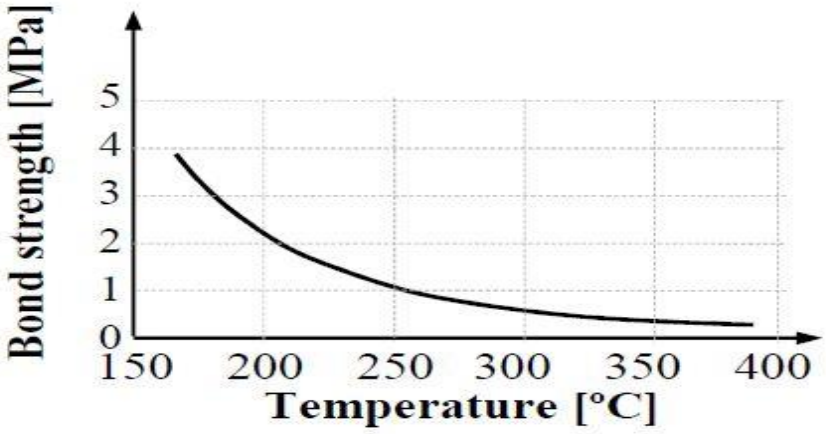

Figure-2.4 Schematic diagram illustrating the bond strength impact of high temperature (Holly et al 2016)

2.3. FLEXURE STRENGTH TESTING OF GFRP BEAMS

Flexure strength also called as bend strength or transverse rupture strength. Flexural strength testing is done in various forms such as one-point load test, two-point load test or uniformly distributed load test force applied perpendicular to the surface of the larger span. By this forms of load setting the material on which load applied starts to bend in opposite to the force applied surface in convex shape by which material experience the tensile stress at the bottom part and compressive stress at the upper part where loads are applied. If a homogenous material is used for flexure testing then it must be good in both tensile and compressive properties the example of this type of substance is steel but it is not economical to make whole sections of steel. Whereas only concrete is tested in the flexure then it is quite weak in tension causing failure at very low strength. So, for removing this problem heterogeneous material is used which is made of steel and concrete. As concrete is good in holding compressive stresses it can be used in the compressive zone and steel is good in holding tensile stresses it will be used in the tension part making RCC a perfect heterogeneous material to be used in construction works. Likewise, in place of steel, GFRP can be used in the tensile zone to cope up with tensile stresses. In one point load test or also called as three-point loading test, a single point is decided to give the load on the structural element, mostly it is chosen at just the centre of the element which is always simply supported on both other supports but some time at the special condition it can be placed at different point rather than middle to obtain some specific result. In two-point loading test or also known as four-point loading test two points at equal distance from the support are chosen to apply load by a non-shear zone is generated between both the point where the load is applied by which elements can be tested for pure flexure force. Likewise, uniformly

distributed load (UDL) test a uniform load is applied at element because in most of the real construction sites UDL is applied on the elements and this can help in making a prototype of structure. Now, for evaluating the flexural strength Benmokrane et al. (1995) have taken 2 different types of GFRP both are made up of E-glass fibre strand (Kdiak and Isorod) and have the similar strength in tension of 689 MPa and elastic modulus of Isorod GFPR is given 42 GPa where Kodiak one ranges from 41 to 50 GPa. With these steel-concrete beams are also cast of the same dimension and same reinforcement to compare the result by them.

Table- 2.1 Characteristic of GFRP beams (Benmokrane et al. 1995)

Series	Height of of beams (mm)	Reinforcement Φ=19.1mm	Beam no.	Compressive strength of concrete (MPa)
1.	300	2 Isorod rebars	ISO30-1	44±2
		2 Isorod rebars	ISO30-2	
		2 Kodiak rebars	KD30-1	
		2 Kodiak rebars	KD30-2	
		2 steel rebars	ST30-1	
		2 steel rebars	ST30-2	
2.	450	2 Isorod rebars	ISO45-1	55±3
		2 Isorod rebars	ISO45-2	
		2 Kodiak rebars	KD45-1	
		2 Kodiak rebars	KD45-2	
		2 steel rebars	ST45-1	
		2 steel rebars	ST45-2	
3.	550	2 Isorod rebars	ISO55-1	43±1
		2 Isorod rebars	ISO55-2	
		2 Kodiak rebars	KD55-1	
		2 Kodiak rebars	KD55-2	
		2 steel rebars	ST55-1	
		2 steel rebars	ST55-2	

The width of all beams is taken as 200mm with a span of 3000mm. All the beams are tested for flexure strength by 4-point load test by applying 5KN force step-by-step with two 200 kN hydraulic jacks. The results of the experiment are discussed in Table-2.2 and are compared with ACI theoretical formulas and overestimation or underestimation of these formulas is discussed.

2.3.1. Check for Ultimate load carrying capacity and load-carrying capacity without crack

Ultimate capacity of carrying load can be defined as the highest load which a sample or material have taken at a point of time on testing under special circumstances. In this ultimate capacities of carrying load were noted in flexural testing of beams. Whereas load-carrying capacity of the material, till it doesn't give any indication of yielding like by giving cracks or other symbols than load at that at time load which is carried by the material, can be called as load-carrying capacity without crack. Now results of the beams of flexure testing are shown below done by (Benmokrane 1995) calculating both ultimate capacity of carrying load and capacity of load carrying without crack.

Table-2.2 Result of the flexure strength test done by the (Benmokrane et al.1995)

Beam no.	$M_{cr\text{-}exp}$	$M_{cr.theor}$	$M_{u\text{-}exp.}$	$M_{u\text{-}theor.}$	Mode of failure
ISO30-1	8.5	11.9	76.7	84.5	shear
ISO30-2	8.5	11.9	80.4	86.0	compressive
KD30-1	9.5	11.9	50.6	79.0	compressive
KD30-2	9.0	11.9	63.8	79.0	compressive
ST30-1	8.5	11.9	79.7	62.7 (78.4)	tensile
ST30-2	8.5	11.9	80.0	63.5 (79.3)	tensile
IS0451	27.0	30.0	102	147.2	shear
ISO45-2	17.0	30.0	122.5	147.2	shear
KD45- 1	25.0	30.0	106.6	137.0	compressive
KD45-2	23.1	30.0	113.0	138.6	compressive
ST45-1	25.0	30.0	103.0	106.5 (133.1)	tensile
ST45-2	25.0	30.0	106.0	106.5 (133.1)	tensile
ISO55-1	36.3	39.7	181.5	184.0	tensile
ISO55-2	35.2	39.7	181.5	182.7	tensile
KD55-1	28.1	39.7	146.9	170.8	tensile
KD55-2	35.0	39.7	172.5	170.8	tensile
ST55-1	36.3	39.7	169.4	131.5 (164.3)	tensile
ST55-2	35.2	39.7	165.0	131.9 (164.8)	tensile

The overall conclusion drawn by the researcher is that GFRP can be utilized as an alternative to steel in the construction site with some strength ratio drawn between GFRP and steel bars which can be used at the time of designing. All the beams with more height of 550mm have failed in tension while beams with less height have shown the mixed type of failures in compression; shear or tension. The first crack values of the beams of the same grade of concrete are exactly the same which shows bonding behaviour of the beams have no difference in GFRP rods and steel rods. The researcher also noticed that formulas which were

given ACI code had overestimated the ultimate moment of the GFRP bars. Another researcher Jabbar and Farid (2018) have done flexure testing on GFRP rebars which were cast by them whose tensile strength was also more than steel and they have tested on small beams of dimensions 100mm x 100mm x 400mm whose results are given in Table-2.3 and Table-2.4.

Table-2.3 Results of tensile strength, bending measurement (Jabbar and Farid 2018)

Strength type	Property	Steel	GFRP
Tensile strength	Yield strength (MPa)	520	593
	Yield strain	17	40
Bending measurement	Yield strength (MPa)	1050	760
	Yield strain	16	20

Table-2.4 Results of compressive strength of concrete (Jabbar and S.B.H. Farid 2018)

Sample type	Compressive strength (MPa)	
	7 days	28 days
Unreinforced concete	20.41	25.67

Results show yield strength in tension of GFRP bars is 13% greater than yield of steel strain 58% higher than steel. Bend strength of GFRP is about 72% of the steel where yield strength is 20% more than steel due to the absence of the perfect behaviour of yielding in the GFRP rods and also it shows that GFRP bars are much weaker in compressive strength because in bending on part of the bar will certainly go to the compression zone. Now flexure strength test is done by the researchers at 7 days and 28 days which are displayed in Table 2.5.

Table-2.5 Flexure test result after 7 and 28 days of the different reinforced beam (Jabbar and Farid)

Property	Days of curing of concrete	Unreinforced concrete	Smooth GFRP reinforced concrete	GFRP coated sand reinforced concrete	Steel reinforced concrete
Strength in	7	2	10.5	11.5	14
flexure (MPa)	28	3	12.5	13.5	17.5
Strain	7	4.5	17	11	8
	28	2	16	10.5	9
Modulus of	7	500	500	1000	2000
elasticity (MPa)	28	1000	500	1000	1500

Yang et al. (2017) had also carried three-point flexure test on GFRP beams; the load is at 250 mm from the support. Tensile test of GFRP, material properties of concrete used and flexure test results details are given in Table- 2.6, 2.7 and 2.8 respectively. Only one rod was used of GFRP of diameter 10 mm so that no other property of any substance can interpret the results.

Table- 2.6 Tensile test result of GFRP bars (Yang et al. 2017)

GFRP bar	Gauge length of extensometer (Le) mm	Ultimate tensile force (F) kN	Strength in tension (fu) MPa	Modulus of Elasticity (E_b) MPa
1	100	88.2	1020	51,900
2		94.8	1100	51,800
3		93.4	1090	50,900
4		96.7	1130	51,700
Mean value		93.3	1090	51,600

Table- 2.7 Properties of concrete (Yang et al. 2017)

Concrete	Strength in compression (f_c) MPa	Strength in tension (f_t) MPa	Modulus of Elasticity (E_c) MPa
1	30.4	2.8	27,100
2	31.9	2.9	28,300
3	29.6	3.2	28,700
4	32.5	3.0	27,900
Mean value	31.1	2.975	28,000

Table-2.8 Three-point flexure test results (Yang et al. 2017)

Bar	Beam abbreviations	Max. crack width (w) mm	Load on time of cracking (P_{cr}) kN	Ultimate load (P_u) kN
GFRP	1	2.33	3	13
	2	1.92	4	12
	3	2.19	4.5	13
	4	2.08	3.5	12
	Mean value	2.13	3.63	12.5
Steel	1	1.60	6	12.5
	2	1.41	5.5	12
	3	1.56	5.7	12
	4	1.47	6.2	11.5
	Mean value	1.51	5.85	12

Where, area of GFRP/steel reinforcement in every beam = 78.5 mm^2, Cross-sectional dimensions (b x h) of every beam = 80mm x 110 mm , with span 1100 mm

Flexure strength test results (Table-2.8) showed that although GFRP has not reached to the strength of reinforced steel concrete but far good results than unreinforced concrete were obtained and also sand coated GFRP give the better result than smooth GFRP. To improve the ultimate capacities of carrying load and cracking load capacity and some other properties which are discussed later Mohamed S. Issa et al. had mixed concrete by different fibres like Polypropylene fibres, Glass fibres and Steel fibre and cast some beams with reinforcement of GFRP. Beam characteristics are given in Table-2.10. The span of beams was taken as 1850mm. The mechanical GFRP bars properties used are given in Table-2.9.

Table-2.9 Mechanical properties of GFRP bars (Issa et al. 2011)

Ultimate tensile strength f_{fu} (MPa)	407.40 of Φ 10 347.50 of Φ 12
Elastic modulus E_f (GPa)	33.81 of Φ 10 32.67 of Φ 12
Rupture strain ε_{fu}	0.029 of Φ 10 0.05 of Φ 12

Table- 2.10 Characteristics of beams (Issa et al. 2011)

Beam no.	Cross sec. dim. *bxt* (mm)	Type of internal fibre	A_s (bott.)	A'_s (top)	Mid. Span stirrups (mm)	Shear span stirrups (/mm)	Target comp. Strength (MPa)
NO	150 × 150	–	3Φ12	2Φ10	–	ϕ8/95	25
HO	150 × 150	–	3Φ12	2Φ10	–	ϕ8/95	65
NP	150 × 150	PP	3Φ12	2Φ10	–	ϕ8/95	25
HP	150 × 150	PP	3Φ12	2Φ10	–	ϕ8/95	65
NG	150 × 150	GF	3Φ12	2Φ10	–	ϕ8/95	25
HG	150 × 150	GF	3Φ12	2Φ10	–	ϕ8/95	65
NS	150 × 150	SF	3Φ12	2Φ10	–	ϕ8/95	25

PP: Polypropylene fibre, GF: Glass fibre, SF: Steel fibre

When flexure strength test is done then results which came out are shown in the Table-2.11. With comparison of ultimate load carrying capacity, cracking load capacity and other parameters researchers came to conclusion that all type of fibres have increased the ultimate load capacity, cracking load capacity and also values given in ACI 440.R1-006 for propylene fibre, glass fibre, steel fibre and all other fibres is really low as compared to the experimental values.

Table-2.11 Test result of various parameters done by (Issa et al. 2011)

Beam no.	Cross sec. dim. (mm)		Type of Internal fibre	Actual comp. strength, f_{cu} (MPa)	A_s (bott.)	A_s' (top)	Test results			
	b	t					Ulti. load (kN)	Deflection (mm)	Cracking load (kN)	Top conc. strain at ulti. load
NO	150	150	–	28.66	3Φ12	2Φ10	39.00	27.49	5.00	0.00307
HO	150	150	–	66.23	3Φ12	2Φ10	52.00	30.56	10.00	0.00415
NP	150	150	PP	39.48	3Φ12	2Φ10	42.00	31.78	11.00	0.00408
HP	150	150	PP	64.28	3Φ12	2Φ10	60.00	35.72	15.00	0.00522
NG	150	150	GF	31.10	3Φ12	2Φ10	56.00	31.71	5.00	0.00498
HG	150	150	GF	54.53	3Φ12	2Φ10	63.00	36.51	11.00	0.00556
NS	150	150	SF	22.98	3Φ12	2Φ10	61.00	45.97	5.00	0.00448

With ultimate load carrying capacity, ultimate strain capacity of beams is also increased significantly by adding steel fibres other fibres addition just give small increment in the strain as shown in Table-2.11. By which we can say overall modulus of elasticity of the composite material has increased to some extent by which can fill the GFRP main drawbacks but corrosion problem remains same due to again use of the steel as fibres in the GFRP-reinforced concrete.

Table-2.12 Result of the ultimate strains both at bottom and top of beams (Issa et al. 2011)

Beam number	Internal fibre type	Ultimate load (kN)	Ultimate strain of top bar ($\varepsilon_u \times 10^{-6}$)	Ultimate strain of bottom bar ($\varepsilon_u \times 10^{-6}$)
NO	–	39.00	200	7 997
HO	–	52.00	753	10 490
NP	PP	42.00	733	10 492
HP	PP	60.00	1269	12 637
NG	GF	56.00	1159	11 295
HG	GF	63.00	–	13 145
NS	SF	61.00	2349	15 815

Cross section all beams are 150mm×150mm.

2.3.2. Deflection

Deflection is the measurement of change in the shape of the material in simple when subjected to some kind of force. The structural component indicates deflection in the direction of force being applied in flexure testing. Material-to-material deflection makes it

materialistic property. Many of the researchers have tried finding the formula for calculating deflection in the flexure testing of beams or other elements. Few of the derived formulas are discussed. The formula for calculating deflection for four-point load test is given as following.

$$\Delta = \frac{PS}{48E_cI_e}(3L^2 - 4S^2) \quad (1)$$

Where,

P is total load, L is the beam span, S is the load distance from the support, E_c is the concrete elasticity module, I_e effective moment of inertia throughout the beam whose different formula is given by various researchers are given below.

According to Benmokrane et al. (1996)

$$I_e = \left(\frac{M_{cr}}{M_a}\right)^3 \frac{I_g}{7} + 0.84\left[1 - \left(\frac{M_{cr}}{M_a}\right)^3\right] I_{cr} \leq I_g \quad (2)$$

Where M_{cr} is the cracking moment, M_a is the moment applied, I_g is the moment of the gross section's inertia, and I_{cr} is the moment of inertia converted into concrete by the cracked section.

According to Brown and Bartolomew (2000)

$$I_e = \left(\frac{M_{cr}}{M_a}\right)^5 I_g + \left[1 - \left(\frac{M_{cr}}{M_a}\right)^5\right] I_{cr} \leq I_g \quad (3)$$

According to Tountaji and Saafi (2000)

$$I_e = \left(\frac{M_{cr}}{M_a}\right)^m I_g + \left[1 - \left(\frac{M_{cr}}{M_a}\right)^m\right] I_{cr} \leq I_g \quad (4)$$

Where $m = 6 - 10\frac{E_{FRP}}{E_S}\rho_{FRP}$ if $\frac{E_{FRP}}{E_S}\rho_{FRP} > 0.3$

Otherwise m=3

According to ISIS design manual M03-1

$$I_e = \frac{I_T I_{cr}}{I_{cr} + \left[1 - 0.5\left(\frac{M_{cr}}{M_a}\right)^2\right](I_T - I_{cr})} \quad (5)$$

Where, I_T is the transformed concrete's un-cracked moment of inertia.

According to ACI 440.1 R06

$$I_e = \left(\frac{M_{cr}}{M_a}\right)^3 \frac{I_g}{7} + 0.84\left[1 - \left(\frac{M_{cr}}{M_a}\right)^3\right] I_{cr} \leq I_g \quad (6)$$

where

$$\beta_d = \frac{1}{5}\frac{\rho_{FRP}}{\rho_{fb}} \leq 1.0 \quad (7)$$

ρ_{fb}= FRP reinforcement ratio of balanced section.

$$\rho_{fb} = 0.85\,\beta_1 \frac{f'_c}{f_{fu}} \frac{E_{FRP}\varepsilon_{cu}}{E_{FRP}\varepsilon_{cu} + f_{fu}} \quad (8)$$

β_1 = factor defining the depth of the rectangular stress block equivalent

f'_c = the cylinder of standard size (150*300mm) strength in compression

f_{fu} = the ultimate strength in tension of FRP bar

ε_{cu} = the ultimate strain in compression of concrete = 0.003.

According to Faza and Ganga Rao determined an articulation for the altered compelling moment of inertia, referred to as I m, for beams subjected to a two-point load scheme. This model relies on the assumption that the concrete section is fully broken between the point loads, while the end sections are broken in portion. The model is organized according to

$$I_m = \frac{23 I_{cr} I_e}{8 I_{cr} + 15 I_e} \quad (9)$$

Where,

$$I_e = \left(\frac{M_{cr}}{M_a}\right)^3 I_g + \left[1 - \left(\frac{M_{cr}}{M_a}\right)^3\right] I_{cr}$$

Where,

$$M_{cr} = \frac{f_r}{y_t} I_g$$

Where,

f_r = rupture modulus

$f_r = 0.62\sqrt{f'_c}$ MPa

y_t = The distance between the centroid and the extreme tensioned concrete fibre.

y_t = h/2.

Benmokrane (1995) attempted to compare the deflections of GFRP beams and steel beams with distinct span-to-height ratios at 50% of the ultimate load shown in Table 2.13.

Table-2.13 Showing deflection at 50% ultimate moment (Benmokrane et al. 1995)

Series no.	Ratio of span to height	50% M_u in kN.m	Deflection of ST-beams in mm	Deflection of ISO and KD beams in mm	Ratio GFRP/steel
1	10.00	35	6.5	25.0	3.85
2	6.67	70	6.5	20.0	2.99
3	5.45	90	5.7	16.1	2.82

As concluded from Table-2.13 span to height ratio deflection of GFRP beams is nearly 4 times which clearly indicating very high GFRP reinforced concrete beams deflection.

Yang et al. (2017) also tested its GFRP reinforced concrete beams for deflection and compared it with the ordinary steel reinforced beams whose results are demostrated in Figure-2.5.

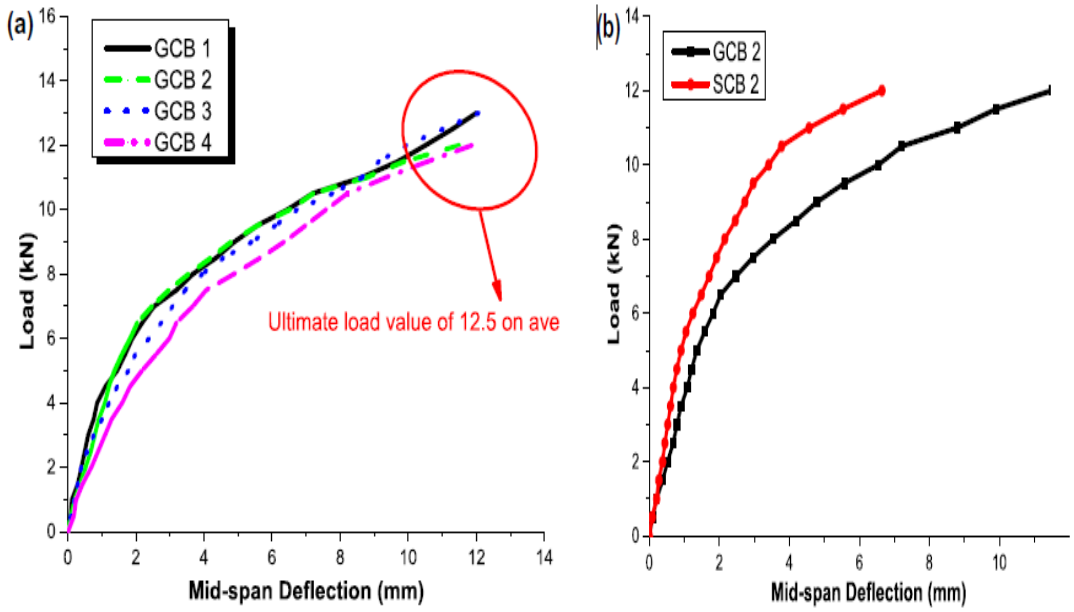

Figure-2.5 Load-deflection curve (a) GFRP beams and (b) comparison steel beam (Yang et al 2017)

Issa et al. (2011) also tested beams whose properties are defined earlier for deflection which is also shown in the Table-2.14, they also tried to find the deflection at service load (they taken service load to that load in which GFRP beam shows deflection is equal to span/180 because yielding point in the GFRP is not defined) and tried to compare with formulas which are given by different researchers for finding deflection.

Table – 2.14 Deflection at service load given by (Issa et al. 2011)

Beam type	Exp. deflection (mm)	Deflection calculated in mm by equation						% error					
		(2)	(3)	(4)	(5)	(6)	(9)	(2)	(3)	(4)	(5)	(6)	(9)
NO	6.43	7.38	6.89	5.18	6.85	6.7	6.61	14.7	7.2	19.5	6.5	4.2	2.8
HO	7.34	9.31	7.72	4.77	8.4	8.48	7.73	26.8	5.2	35.0	14.4	15.6	5.3
NG	9.59	10.5	10.4	9.01	10.1	10.2	10.0	9.8	8.2	6.1	5.6	6.0	4.3
HG	8.65	11.4	10.9	8.37	10.8	10.9	10.4	31.9	26.4	3.2	24.8	26.5	19.7
NP	5.72	7.77	6.89	4.72	7.09	7.06	6.71	35.8	20.5	17.4	24.0	23.4	17.3
HP	7.12	10.8	9.85	6.8	9.99	10.1	9.38	51.1	38.4	4.5	40.3	42.5	31.7
NS	11.5	11.7	11.7	10.9	11.5	11.5	11.5	2.3	1.9	4.5	0.10	0.26	0.26
Average % error								24.6	15.4	12.9	16.5	16.9	11.6
Standard % deviation								15.6	12.4	10.9	13.0	13.9	10.7
Variation coefficient (ratio)								0.63	0.81	0.85	0.79	0.82	0.92

Table-2.15 Deflection at 1.3 times service load (Issa et al. 2011)

Beam type	Exp. deflection (mm)	Deflection calculated in mm be equation (mm)						%error					
		(2)	(3)	(4)	(5)	(6)	(9)	(2)	(3)	(4)	(5)	(6)	(9)
NO	9.5	9.6	9.42	8.05	9.19	9.18	9.06	1.1	0.8	15.3	3.2	3.4	4.6
HO	11.11	12.08	11.4	8.42	11.38	11.6	10.8	8.7	3.0	24.2	2.4	4.1	2.7
NG	13.35	13.68	13.6	12.7	13.37	13.5	13.3	2.5	2.1	4.9	0.2	0.8	0.1
HG	12.25	14.85	14.7	12.8	14.37	14.6	14.1	21.2	19.8	4.1	17.4	18.9	15.3
NP	8.37	10.08	9.74	7.78	9.56	9.64	9.28	20.4	16.4	7.0	14.2	15.1	10.9
HP	10.46	13.98	13.6	11.1	13.4	13.6	13.0	33.7	30.5	5.7	28.1	30.1	24.0
NS	16.07	15.24	15.2	14.8	15.03	15.1	15.1	5.2	5.3	8.1	6.5	6.2	6.2
Average (%) error								13.3	11.1	9.9	10.3	11.2	9.1
Standard (%) deviation								11.2	10.5	6.8	9.4	9.8	7.7
Variation coefficient (ratio)								0.84	0.94	0.68	0.91	0.88	0.85

2.3.3. Ductility

The ratio of ultimate deformation to yield deformation can be described as ductility. Due to low elasticity modulus and linear brittle behaviour GFRP beams have very less ductility than steel beams. As recommended by ACI.440.1R-06, it is necessary to design FRP-reinforced concrete beams over reinforced so that concrete fails first and then GFRP bar breaks. As yield point of the GFRP cannot be found due to elastic behaviour throughout stress-strain graph, so Vijay and Ganga Rao told that FRP ductility is evaluated by means of the deformability factor (DF), defined as the ratio of the ultimate energy absorption (area under the load-deflection curve to the ultimate load) to the energy absorption at the service load (at the

span/180 serviceability deflection limit). Deformability factor of above beams created by M. S. Issa et al. (2011) is given in Table-2.16.

Table-2.16 Deformability factors of beams (Issa et al. 2011)

Beam code	Type of fibre/volume ratio %	f_c' (MPa)	ρ_f %, (FRP bars)	DF	Increase in DF compared to non-fibrous FRP beam (%)
NO	No fibre	22.93	1.87 GFRP	3.60	–
HO	No fibre	52.98	1.87 GFRP	5.90	–
NP	PP/0.5	31.58	1.87 GFRP	6.00	66.70
HP	PP/0.5	51.42	1.87 GFRP	8.70	47.50
NG	GF/0.5	24.88	1.87 GFRP	7.70	113.9
HG	GF/0.5	43.62	1.87 GFRP	11.30	91.50
NS	SF/0.5	18.38	1.87 GFRP	13.60	277.8

2.4.OBSERVATIONS AND GAPS KNOWN FROM THE LITERATURE REVIEW

Following are the observations and gaps after critically analysing the literature review:

1. The application of GFRP bars in the construction industry is a good alternative to conventional steel bars, because of low unit weight, non-corrosive property, less cost. The manufacturing parameters of GFRP bars responsible for its higher tensile strength are type of glass fibre, type of resin, manufacturing technique and temperature. No special codes are available which helps to maintain the same production quality of the GFRP bars.
2. The surface quality of the GFRP bar and other conditions like temperature and chlorinated environment affects the bond properties between the GFRP and concrete.
3. Flexural strength of GFRP reinforced concrete beam has little low experimental results then steel when tested at same reinforcement ratio, whereas there is clash of interest between researchers on difference between theoretical and experimental values of beams, few conclude that ACI 440 code predict more than the experimental ultimate carrying capacity while some other conclude that calculated ultimate carrying capacity was lesser than experimental one. Also no comparisons are made by equating the ultimate moments of both the beams.
4. The main problem GFRP reinforced concrete beam face is high deflection due to low modulus of elasticity. Deflection is calculated by the different formulas by researcher. Every formula satisfy experimental deflection up to some extent but which one have more precision cannot be concluded from the given data of research papers.

5. GFRP beams are advised to designed over-reinforced by researchers so that concrete will fail first, because if GFRP fails first then abrupt failure due to elasticity modulus. But if low modulus of elasticity is reason for over-reinforcement design then first de-bonding will occur by concrete which will give ample warning before failure.

2.5. OBJECTIVES OF THE PRESENT WORK

The objectives of the work are briefly discussed in this section:

1. ACI440 will be used to calculate the ultimate capacity of the GFRP beams which will be compared with experimental ultimate-carrying capacity and after steel beams of same ultimate-moment carrying capacities are designed and then difference in the ultimate-moment carrying capacity will be calculated.
2. The deflection of the beams will be found experimentally and then compared with the calculated values by the given formulas in ACI440 and IS 456.
3. Load-deflection graphs are drawn with the help of experimental data and then comparison are made between the behaviour of steel and GFRP-Steel beam.
4. Ductility of steel beams are calculated by the help of ultimate deflection and first crack deflection and will be compared with ductility of GFRP-Steel beams found by same process as steel beams.
5. Energy absorption of beams are found with help of the area under the load-deflection graphs and then comparison will be made between equal ultimate load-carrying capacity GFRP-Steel and steel beam.

CHAPTER – 3

EXPERIMENTAL METHODOLOGY

3.1. GENERAL

The chapter describes the materials properties of ordinary Portland cement, coarse, fine aggregates, GFRP rebars and steel rebars which are used to prepare beams. Physical properties like fineness, specific gravity, water absorption and final and initial setting time are in the range of the relevant test standards. With the help of this properties mix design proportion is calculated and cubes are prepared for testing strength in compression of concrete.

3.2. MATERIALS

3.2.1. Ordinary Portland Cement (OPC 43)

Shree-ultra cement OPC 43 is the cement used for the current work. It is shielded from humidity to avoid its characteristics from deteriorating. Specific gravity, fineness, initial and final setting time are the distinct tests performed on cement. The physical properties of the cement are shown in Table 3.1 and are verified by IS codes that are permissible.

Table 3.1 Properties showing physical behaviour of cement

Properties	Obtained values	IS codes values permissible
Specific gravity	3.13	Between 3.1 to 3.16
Fineness of cement (% retained on 90 μm sieve)	5.9	Maximum 10%
Setting time (initial)	70 minutes	Minimum 30 minutes
Setting time (final)	450 minutes	Maximum 600 minutes

3.2.2. Coarse Aggregates

Coarse aggregates utilized in present work are of two sizes maximum size of 20 mm and maximum of 10 mm size used in the proportion of 6:4 respectively. The aggregates are cleaned and made soil-free before performing the experiment to determine their physical characteristics. Specific gravity, water absorption and sieve analysis are the different properties tested. The results obtained are presented in Tables 3.2 and 3.3.

Table 3.2 Coarse aggregate physical properties (60% of the largest size 20mm and 40% of the largest size 10mm)

Physical properties	Values obtained
Specific gravity	2.6 (approx.)
Water absorption	0.91%
Colour	Multi-colour (red, black, blue, white etc.)

Table 3.3 Coarse aggregate fineness modulus (60% of the largest size 20mm and 40% of the largest size 10mm)

Sieve	Retained weight (gm)	Retained percentage	Cumulative retained weight (%)
40	0	0	0
20	221	4.55	4.55
10	3444	71.01	75.56
4.75	1027	21.17	96.73
Pan	171.5	8.54	100.00

Total weight taken= 4850 gm

Fineness modulus of coarse aggregate = 6.76

3.2.3. Fine Aggregate

Fundamentally, fine aggregates are sand obtained from land or marine origin. Fine aggregates consist of smaller or larger sand or crushed stone particles with the majority of particles passing through a sieve of 4.75 mm. The sand used in this work is river sand obtained from Pathankot, Punjab. Specific gravity, water absorption and sieve analysis refer to Figure 3.1 are the distinct characteristics assessed. The outcomes of tests are provided in Table 3.4 and 3.5.

Table 3.4 Fine aggregate physical properties

Physical properties	Values obtained
Specific gravity	2.68
Absorption of water	3.21%
Zone	II
Colour	Light grey

Figure 3.1 Weight of oven dried fine sand

Table 3.5 Fine aggregate fineness modulus

Sieve	Retained weight (kg)	% of weight retained	Cumulative weight retained (%)
4.75	0	0	0
2.36	0.101	12.46	12.460
1.18	0.173	21.35	33.810
0.6	0.068	8.395	42.205
0.3	0.2	24.691	66.686
0.15	0.214	26.79	93.686
Pan	0.043	5.30	98.986

Total weight taken = 0.810 kg.

Fineness modulus of fine aggregate = 2.49

3.2.4. Steel Rebars

The steel used in the present experiment is Fe 500 according to Indian code (IS-1786:2008) which have a carbon percentage of nearly 0.25% to 0.30% varies from producer to producer. The properties of bars of 8 mm and 10 mm diameters are presented in Table 3.6.

Table 3.6 Strengthening properties of Fe500 steel (IS-1786:2008)

Parameter	Value
Stress at yield (N/mm^2)	500
Ultimate strength in tension (N/mm^2)	560
Maximum elongation (%)	16%

3.2.5. GFRP Rebars

In this experiment setup bar of 8mm, 10mm and 16 mm are used shown in Figure 3.2 because of the rapid availability. Every different diameter has different tensile strengths which are shown in Table-3.7 given by Xian Kig Technology Company, China. The elastic modulus of GFRP is nearly 60000 MPa. GFRP is much more resistant to the corrosion than the steel.

Table 3.7 Strength in tension of different diameter GFRP bars (Provided by manufacturer)

Diameter in mm	Strength in tension (MPa)
8	1080
10	980
16	752

Figure 3.2 GFRP bars of different diameters

The weight of the GFRP is much lighter than the steel as presented in Table 3.8.

Table 3.8 Comparison of the weight of steel and GFRP rebars

Diameter in mm	Weight of steel (kg/m) as per IS-1786:2008	Weight of GFRP (kg/m) as given by manufacturer
8	0.395	0.106
10	0.617	0.165
16	1.578	0.323

3.3. MIX DESIGN

The concrete is prepared to attain specific compressive strengths of M30 and M35 as per IS-10262:2009. M30 and M35 grade of concrete is used because lots of researcher reported that GFRP bars bonding properties are good in the higher grade concretes, so grade M30 and M35 are highest grades as per IS-10262:2009, which can be prepared with the normal constructional above mentioned materials without using the special plasticizers or other chemicals. According to IS-10262:2009, M30 will give characteristic strength of 38.25MPa and M35 will give characteristic strength of 43.25MPa. The mix design ratios of M30 and M35 are presented in Table 3.9.

Table 3.9 Mix design for M30 and M35

Concrete Grade	Water-cement ratio	Cement (kg/m^3)	Coarse aggregate largest size 20 mm (kg/m^3)	Coarse aggregate largest size 10mm (kg/m^3)	Fine aggregate (kg/m^3)	Water (kg/m^3)
M30	0.4	492.5	655.69	437.13	606.51	197
M35	0.35	562.85	642.79	428.53	586.86	197

After mix design the concrete cubes are cast by creating the above-mentioned mixes in a specific quantity so that mix can fill 2 cubes of dimension 150mm×150mm×150mm for every concrete grade. Two cubes are made which are then tested at an interval of 7days. The first trial of seven days are made as shown in Figure 3.3 whose result is shown in Table 3.10 is done with the use of compressive testing machine (CTM) whose maximum capacity is 5000kN and loading rate applied is 5kN/second as shown in Figure 3.4.

Table 3.10 First trial test of 7days cubes in CTM

Concrete grade	Compressive load (kN)	Stress in compression (N/mm^2)	Average of Stress in compression (N/mm^2)
M 35	586.0	26.04	22.62
	432.2	19.20	
M 30	254.2	11.20	9.75
	177.8	7.80	

Figure 3.3 Cube samples in moulds

Figure-3.4 Strength testing of a cube in CTM (compressive)

The first trial is unable to give expected results due to a lack of precision or other factors. So again trials are made and tested with more precision. The result of the second trial is shown in Table 3.11 which showed some satisfying results.

Table 3.11 Second test trial of 7days cubes in CTM

S.No.	Concrete Grade	Compressive load (kN)	Stress in compression (N/mm^2)	Average of Stress in compression (N/mm^2)
1.	M 35	619.4	27.52	24.03
		555.6	20.54	
2.	M 30	333.6	14.82	17.29
		444.7	19.77	

After successful 7 days trial 3 cubes of each grade of concrete for 28 days are cast and for compression testing. The result of the trial is shown in Table 3.12.

Table 3.12 Test trial of 28days cubes in CTM

S.No.	Concrete Grade	Compressive load (kN)	Stress in compression (N/mm^2)	Average of Stress in compression (N/mm^2)
1.	M 35	695.6	30.91	31.76
		740.2	32.89	
		708.4	31.48	
2.	M 30	854.3	37.96	37.96
		791.2	35.16	
		899.2	39.96	

3.4. CASTING PROCEDURE OF BEAMS

After getting some satisfying result in the compressive testing in 28days, 3 cubes of each grade are prepared for checking compressive strength after 28 days with every 8 beams of steel and GFRP-Steel beams. The results of the compressive test are discussed in Table 3.12.

Table 3.13 Testing results of 28 days cubes in CTM

S.No.	Concrete Grade	Beam type	Compressive load (kN)	Compressive stress (N/mm^2)	Average of Compressive stress (N/mm^2)
1.	M 30	Steel	706.5	31.4	31.5
			688.5	30.6	
			731.2	32.5	
2.	M 30	GFRP-Steel	663.7	29.5	30.1
			668.2	29.7	
			699.7	31.1	
3.	M 35	Steel	929.2	41.3	40.2
			893.2	39.7	
			892.2	39.6	
4.	M 35	GFRP-Steel	858.0	38.1	36.9
			851.2	37.8	
			787.4	.34.9	

3.4.1. Configuration of Steel bars and GFRP bars in Beams

Thirty-two are beams of span length 700mm, 150mm depth and 150mm width cast in two series:

- Series-1 consists of 16 steel RC beams using conventional steel Fe500 are prepared.
- Series-2 consists of 16 beams containing GFRP bars of main longitudinal tensile reinforcement and with steel bars as main longitudinal compressive bars.

Firstly, Series 2 beams were created with 4 different reinforcement configurations which are discussed below in Table 3.13 and then series-1 beams were created by finding the area of steel which can give same ultimate moment capacities which was given by 4 configurations of series-2 beams respectively. Every main bar whether series-1 or series-2 is cut into 670mm so that cover at least 15mm will be left on each of beam. Stirrups in every beam are of 2-legged 8mm diameter of dimension 115mm×115mm at the space of 60mm centre to centre. The minimum concrete cover of 15mm is provided at every side of the beam.

Table 3.14 Different reinforcement configuration of series-2 beams

Name given to the beam	Number of upper bars (steel)	Diameter of upper bars (mm)	Number of lower bars (GFRP)	Diameter of lower bars (mm)	GFRP bar % reinforcement ratio of beam
G1	2	8	3	8	0.67
G2	2	8	3	10	1.05
G3	2	8	2	16	1.78
G4	2	8	3	16	2.68

For each configurations two similar beams are cast making them 8 beams, likewise, these beams are created in two concrete grades M30 and M35 making them to 16 beams. Moments of these of configuration are calculated according to ACI 440.1R-06 and for that moment Steel beams were designed with help of IS456-2000 and newly derived formula (without partial safety factors shown in Annexure-A) with minimum error possible shown in Annexure B and C. Table 3.14 were the arrangements which are made of steel beams. Cross-section of beams compared with each other is discussed from Figure 3.4 to 3.7 with help of sketches.

Table 3.15 Different reinforcement configuration of series-1 beams

Name given to the beam	Number of upper bars (steel)	Diameter of upper bars (mm)	Number of lower bars (steel)	Diameter of lower bars (mm)	Steel bar % total reinforcement ratio
S1	2	8	3	8	1.12
S2	2	8	2	12	1.45
S3	3	8	3	12	2.18
S4	3	12	3	12	3.01

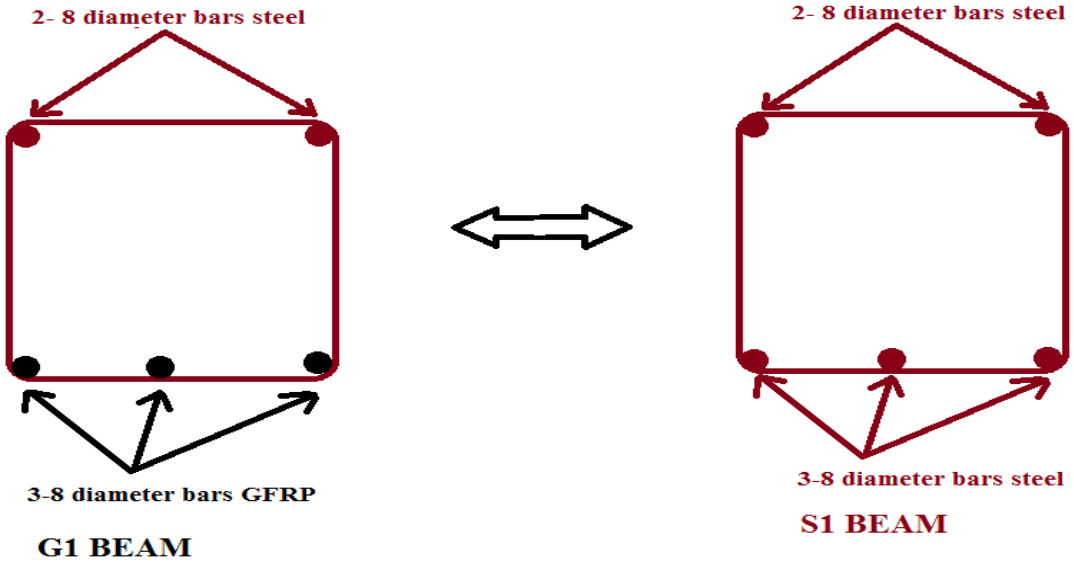

Figure 3.5 Sketch representing reinforcement placement of S1 and G1 beam

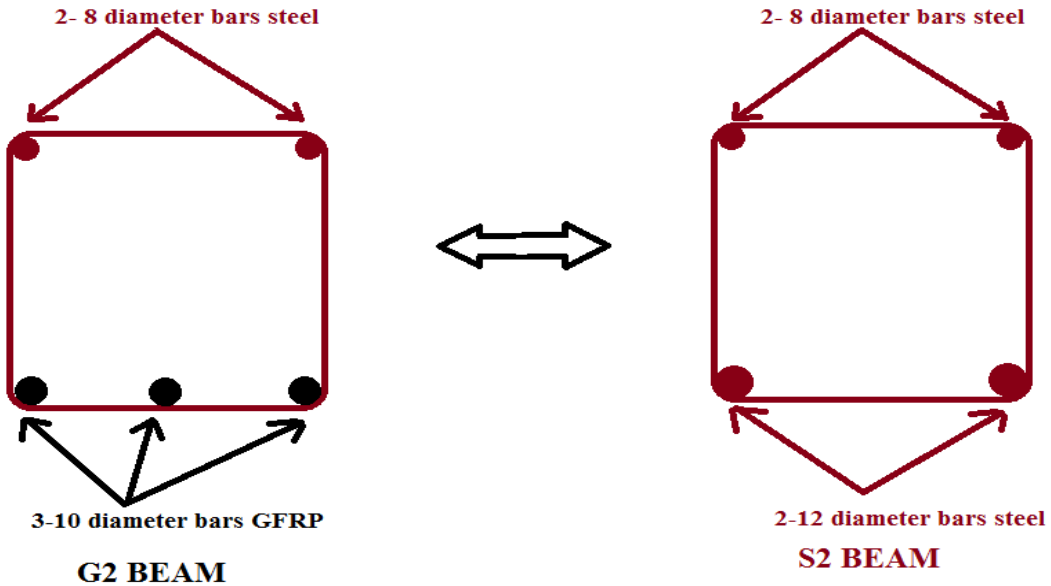

Figure 3.6 Sketch representing reinforcement placement of S2 and G2 beam

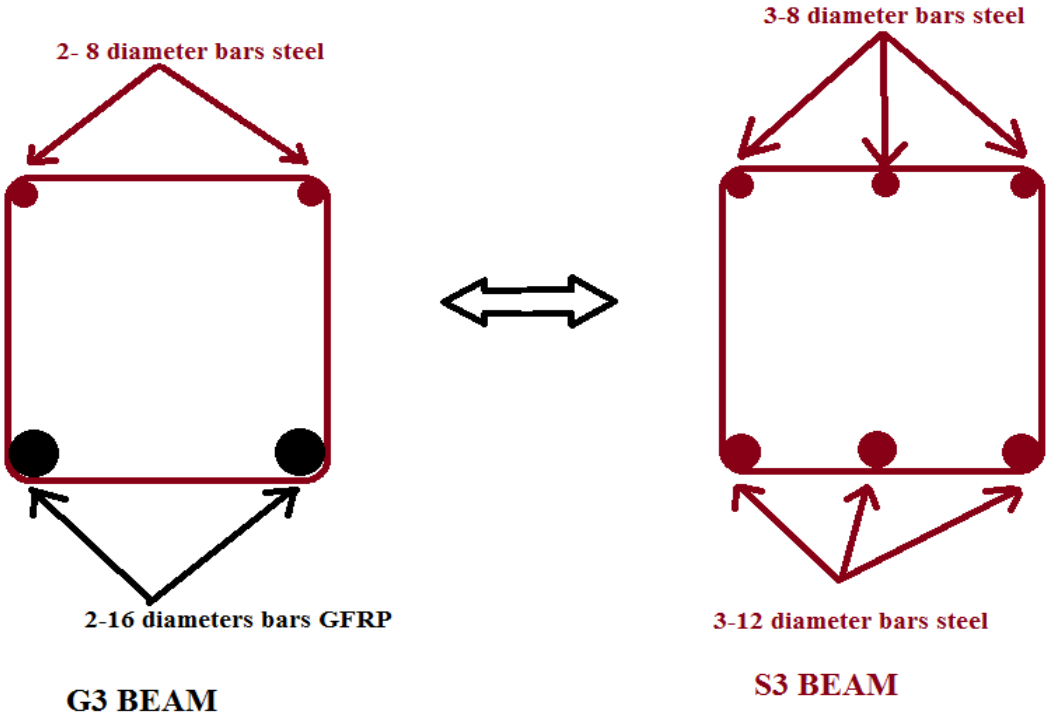

Figure 3.7 Sketch representing reinforcement placement of S3 and G3 beam

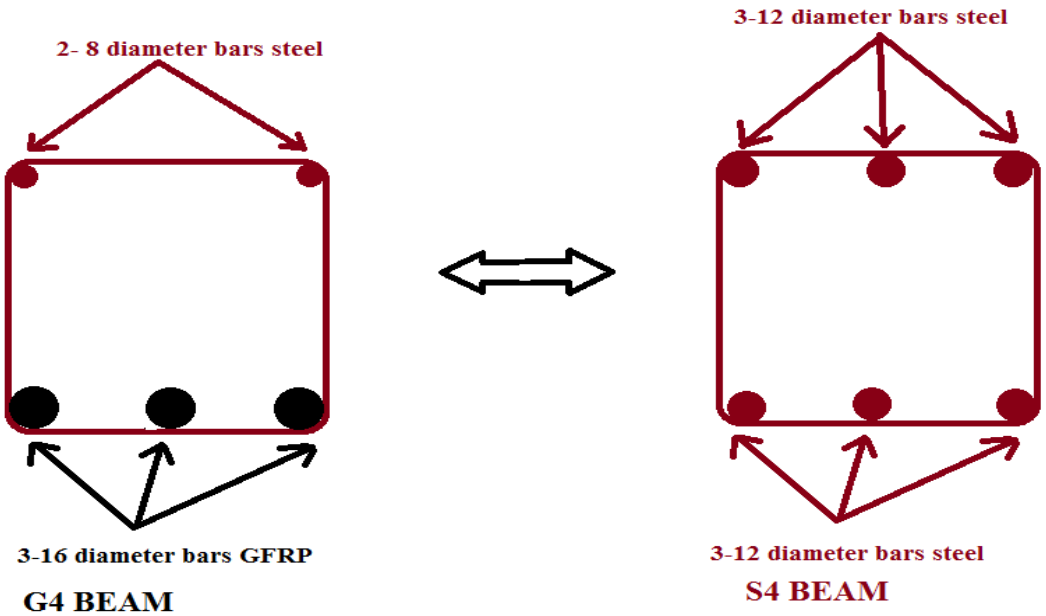

Figure 3.8 Sketch representing reinforcement placement of S4 and G4 beam

3.4.2. Casting of Beams

Concrete is hand mixed for 4 beams at a time. After casting all the beams are placed in plastic drums full of water for 28 days curing. After which these beams tested according to two-point loading test which will be discussed in a further section 3.4. Pictures of the whole process were shown in Figure 3.8 to 3.11.

Figure 3.9 Steel and GFRP arrangements of beams

The long bars of nearly 12 meters cut into a small piece of 670mm for the long main reinforcement. Shear stirrups piece of 500 mm are cut and then bend 500 at 4 places to make a stirrup of dimension 115mm×115mm. Afterwards, stirrups and main reinforcements are tied up together with the help of steel wires in the different configuration as mention section 3.3.1 by which steel reinforcement arrangements are formed as displayed in Figure 3.8.

Figure 3.10 Oiled moulds with Steel and GFRP arrangements of beams

After preparations of the steel and GFRP configurations of beams, the moulds of dimension 700mm×150mm×150mm are available in the structure lab were tightened with help of spanner and then oiled with the spare mechanic oil with the help of paintbrush which is shown in Figure 3.9. After oiling the steel and GFRP arrangements are placed in the moulds in a specific manner that concrete cover of 15mm will be left at every face of the mould. After placing skeletons concrete which is prepared as per the mix designed concrete is placed in the mould and then compacted with the help of vibrator present in the structure lab.

3.4.3. Curing Procedure of Beams

Figure 3.11 Beam specimens after dismantling

After compacting concrete, moulds are left for 24 hours for curing of concrete. After 24 hours, the beams are placed out of the moulds by losing the moulds with the help of spanner. Beams which are out of moulds are shown in Figure 3.10.

Figure 3.12 Prepared beams were placed in plastic tanks for 28 days curing.

Beams are then placed in the PVC plastic drums and then plastic drums are filled with freshwater as shown in Figure 3.11 and beams are left for curing for 28 days. Water level is maintained with after 2-3 days in by refilling between 28 days of curing.

3.5. EXPERIMENTAL SETUP FOR TESTING BEAMS

Beams are tested in two-point loading with help of UTM (Universal Testing Machine) of capacity 3000kN with special arrangements as represented in Figure 3.8 at a loading rate of UTM is 0.1kN/sec. At the mid-span of the beam, a digital dial gage with a precision of 0.001 mm is used to verify deflection. The readings of deflection from dial gauge are recorded after every unit rise in load and using these values load-deflection curves are made.

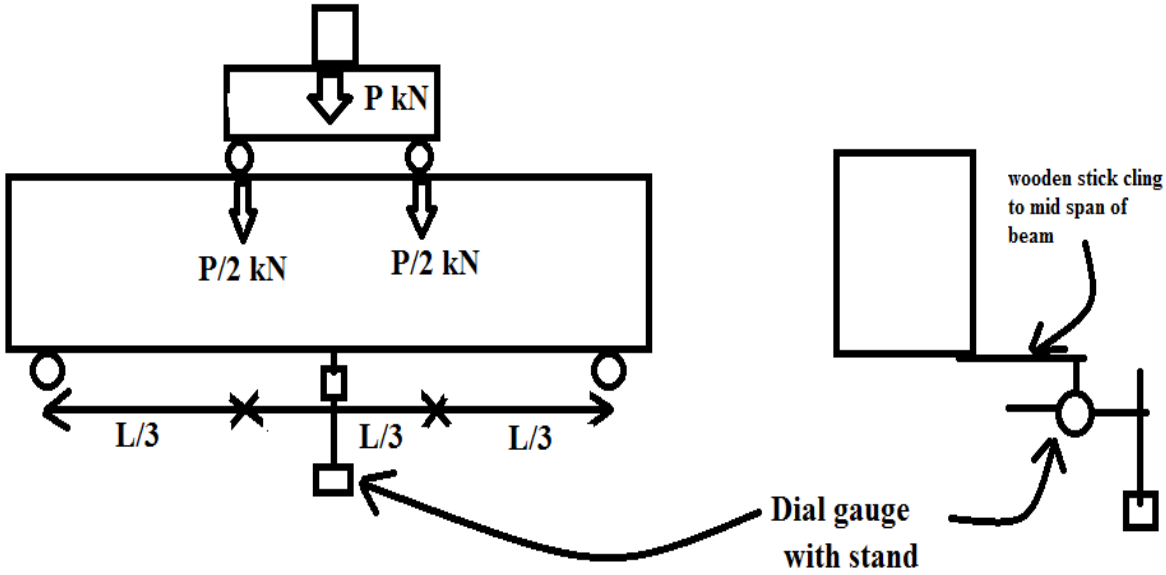

Figure3.13 Experimental setup for testing beam in two-point loading test

In Figure 3.13, total L is 600mm. Loads are applied on L/3 from every support. Simple supports are placed at 50mm from the lower edge of the beam each side. This arrangement will make the middle L/3 part with zero shear force that is only constant moment will work on the part which gives the probability of failing beam in pure flexure behaviour in middle. The shear force (V) and moment (M) will be generated under the application of loads is explained by with the help of sketch in Figure 3.9. After the selection of arrangement, all 32 beams are tested with this arrangement and then experimental results are obtained by applying loads.

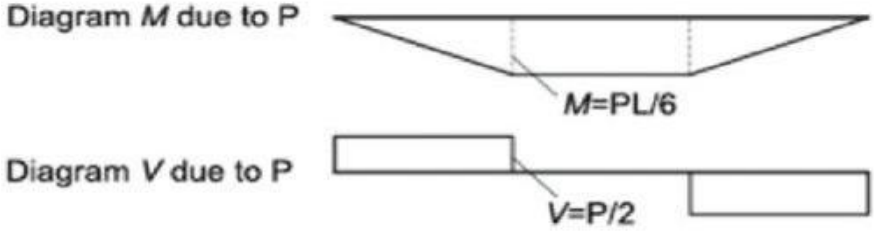

Figure3.13 Bending moment and Shear force under two-point load arrangement

If it is assumed that P is the reaction which is generated on the machine upper part which is then distributed as P/2-P/2 by the arrangement made on the UTM as shown in Figure 3.8 which will cause maximum constant moment of PL/6 and Zero shear force in middle L/3 section and on the other both L/3 sections a linearly increasing moment from zero to PL/6 from support to middle L/3 section can be seen whereas constant P/2 shear force will be generated. Value of P will be shown on UTM by which shear force and bending moment can be calculated. The value of shear will directly give the value load which is carried by the beam and bending moment will give value of the moment which is generated on the middle L/3 section these values will help us in fetching the ultimate load and capacity of carrying moment the beam. Likewise ultimate mid-span deflection and deflection at first crack will be recorded by the help of dial gauge fitted at lower mid-span of beam as presented in Figure 3.12. Ductility of beams is calculated by calculating the ratio of ultimate deflection and first crack deflection. Energy absorption of beams is calculated as the area under the load-deflection curve. Crack patterns of the beam are observed throughout the process of applying load every single crack is marked from generation to end of its propagation.

CHAPTER-4

RESULTS AND DISCUSSION

4.1. GENERAL

The main objective to present work is to compare the steel-RC beams and GFRP-Steel beams in terms of capacity of load carrying, deflection, ductility, energy absorption and crack-pattern to know the acceptability of GFRP bars in the constructional use. Flexural properties of all the beams are tested in the two-point loading. Following sections discuss the test results of the investigated properties.

4.2. ULTIMATE MOMENT CAPACITY OF BEAMS

Beams are tested on the basis of arrangement discussed in section 3.4 and their ultimate failure moments are calculated by getting the ultimate force of every beam arrangement. After averaging the experimental ultimate failure load of similar beams will be compared by the calculated ultimate failure load of the respective beams. Calculated ultimate moments are calculated with the help of formulas which are given in IS 456:2000 for Steel-RC and ACI440.1R-06 for GFRP-RC beam.

4.2.1. Calculated and Experimental Values of Ultimate Forces and Moments of Steel Beams

When under-reinforced beams are calculated then the experimental ultimate load values and calculated ultimate load values have a huge difference in them. This difference is generated due to the use of partial safety factors of materials in the code. So, to nullify the gap of ultimate values new formulas are derived without material partial safety factors shown in Annexure-A. Calculated values with new formulas are quite near to the experimental values, calculations are shown in Annexure-B. Doubly-reinforced beams calculated ultimate load values are found by fixing the neutral axis where the tensile and compressive forces are equal which gave ultimate load calculated values which are very near to experimental ultimate load values calculations are shown in Annexure-C. Calculated, experimental and % error values of steel beams are presented in Table 4.1, 4.2 and 4.3 respectively.

Table 4.1 Calculated ultimate forces and moments of M30 and M35 steel beams.

Beam No.	Calculated ultimate force values M30 (kN)	Calculated ultimate moment values M30 (kN-m)	Calculated ultimate force values M35 (kN)	Calculated ultimate moment values M35 (kN-m)
S1	48.23	9.64	48.75	9.75
S2	57.48	11.49	70.42	14.08
S3	81.85	16.37	84.58	16.91
S4	88.27	17.65	90.81	18.16

Table 4.2 Experimental ultimate forces and moments of M30 and M35 steel beams.

Beam No.	Averaged experimental ultimate force values of M30 beams (kN)	Averaged experimental ultimate moment values of M30 beams (kN-m)	Averaged experimental ultimate force values of M35 beams (kN)	Averaged experimental ultimate moment values of M35 beams (kN-m)
S1	47.58	9.51	51.2	10.24
S2	63.59	12.72	68.32	13.66
S3	79.97	15.99	90.04	18.01
S4	84	16.8	93.82	18.76

Table 4.3 % error between experimental and calculated values of ultimate force of M30 and M35 steel beams

Beam No.	%error in M30 beams	%error in M35 beams
S1	1.34	5.00
S2	10.64	2.98
S3	2.29	6.44
S4	4.83	3.31

No specific error pattern can be concluded from the percentage of errors in relation to the reinforcement ratio, but the experimental and calculated ultimate load or moment have much less error.

4.2.2. Calculated and Experimental Values of Ultimate Forces and Moments of GFRP-Steel Beams

Ultimate capacities of load carrying of GFRP-Steel beams are calculated with the help of ACI440.1R-06. Tensile strengths of GFRP bars are taken which are given by the manufacturer. Nominal capacity of moment of the beam is considered not the actual strength which will come after multiplying the reduction factor. Calculation of the ultimate moment of GFRP-Steel beams is shown in Annexure-B and also in Annexure-C. Calculated, experimental and % error values of M30 and M35 GFRP-Steel beams are presented in Table 4.4, 4.5 and 4.6 respectively.

Table 4.4 Calculated ultimate forces and moments of M30 and M35 GFRP-Steel beams.

Beam No.	Calculated ultimate force value of M30 beams (kN)	Calculated ultimate moment value of M30 beams (kN-m)	Calculated ultimate force value of M35 beams (kN)	Calculated ultimate moment value of M35 beams (kN-m)
G1	53.92	10.78	55.41	11.08
G2	62.72	12.54	65.87	13.17
G3	68.52	13.70	75.57	15.11
G4	77.76	15.55	86.26	17.25

Table 4.5 Experimental ultimate forces and moments of M30 and M35 GFRP-Steel beams.

Beam No.	Averaged experimental ultimate force values of M30 beams (kN)	Averaged experimental ultimate moment values of M30 beams (kN-m)	Averaged experimental ultimate force values of M35 beams (kN)	Averaged experimental ultimate moment values of M35 beams (kN-m)
G1	54.72	10.94	53.12	10.62
G2	65.46	13.09	58.09	11.61
G3	67.2	13.44	69.92	13.98
G4	67.98	13.59	82.28	16.45

Table 4.6 % error between experimental and calculated values of the ultimate force or moment of M30 and M35 GFRP-Steel beams

Beam No.	%error in M30 beams	%error in M35 beams
G1	1.47	4.12
G2	4.37	11.80
G3	1.92	7.48
G4	12.57	4.61

In GFRP-Steel beams also there is no specific pattern in the % error of beams with reinforcement ratio but GFRP-Steel has more percentage error in experimental and calculated ultimate load or moment than the steel beams.

4.2.3. Comparison between Control Beams and GFRP-Steel Beams on Ultimate Load-Carrying Capacity

When the calculation of the GFRP-Steel beams G1, G2, G3 and G4 and the steel beams S1, S2, S3 and S4 is seen errors comes up in both M30 and M35 which is shown in Table 4.7.

Table 4.7 % error in moment values when calculated of M30 and M35 beams when compared with each other

Beams compared on the basis of calculation		% error in values of M30 beams	% error in values of M35 beams
G1	S1	13.05	10.56
G2	S2	2.85	8.36
G3	S3	19.01	19.45
G4	S4	23.55	13.05

As calculated moments shows some errors in the compared beams likewise in the experimental data some of the errors can be seen in the compared beams which are shown in the Table 4.8, afterwards difference in the errors are compared between the calculated and experimental data in Table 4.9.

Table 4.8 Error in moment values when experimentally observed of M30 and M35 beams when compared with each other.

Beams compared on the basis of the experimental obtained value		% error in values of M30 beams	% errors in values of M35 beams
G1	S1	10.56	12.00
G2	S2	8.36	6.91
G3	S3	19.45	11.91
G4	S4	13.50	5.27

Table 4.9 Difference in the calculated and experimental errors in the M30 and M35 beams.

Beams compared	Difference between both %errors in M30 beams	Difference between both %errors in M35 beams
G1 and S1	2.48	8.38
G2 and S2	5.50	10.69
G3 and S3	0.44	16.85
G4 and S4	10.04	8.74

4.3. MID-SPAN DEFLECTION IN BEAMS UNDER TWO-POINT LOAD TEST

As known deflection of every beam was noted up to the ultimate load corresponding to which experimental deflection can be compared with the calculated deflection whose formula is described in ACI440.1R-06 for GFRP beams and for steel following formula is used for calculating the theoretical deflection.

$\Delta_{max} = \frac{Pa}{24E_cI_{eff}}(3L^2 - 4a^2)$ (structx.com/Beam_Formulas_009.html)

Where,

Δ_{max} = At the mid-span maximum deflection of the beam.

P is equal load acting on two points of the beam.

a is the length from support to load point.

L is the beam span

E_c is the modulus of elasticity of concrete can be calculated as $E_C = 5000\sqrt{f_{ck}}$ according to IS456:2000.

I_{eff} is effective moment of inertia can be calculated by the formula $I_{eff} = \left(\frac{M_{cr}}{M_a}\right)^3 I_g + \left[1 - \left(\frac{M_{cr}}{M_a}\right)^3\right] I_{cr}$ (ACI440.1R-06)

Where

M_a is th real moment of the beam.

$M_{cr} = \frac{f_r}{y_t} I_g$

I_g is the gross moment of inertia of total section (when all section is considered of concrete)

$f_r = 0.7\sqrt{f_{ck}}$

y_t is the line which divides the section into two equal-area parts.

I_{cr} is the second moment when the section is considered homogenous material.

Deflection of both beam steel and GFRP-Steel is shown in Annexure-D.

4.3.1. Calculated and Experimental Values of Mid-Span Deflection of Steel Beams

Steel beams deflections are discussed with experimental known and theoretically calculated values and then error between them are discussed. Experimental moments are taken for calculation of deflections. Experimental and calculated deflections are compared with steel beams in Table 4.10.

Table 4.10 Mid-span deflection comparisons calculated versus experimental of M30 and M35 steel beams

Beam No.	Calculated deflection of the M30 beams	Experimental deflection of the M30 beams	Calculated deflection of the M35 beams	Experimental deflection of the M35 beams
S1	1.241	1.242	1.302	1.305
S2	1.261	1.264	1.289	1.298
S3	1.186	1.187	1.287	1.291
S4	1.245	1.253	1.341	1.346

4.3.2. Calculated and Experimental Values of Mid-Span Deflection of GFRP-Steel Beams

The real experimental values of both the beams are taken and then deflection is calculated by the formula given in the ACI 440.1R. Deflections of the GFRP-Steel beams are much higher than the steel beams which can make a building unserviceable. Deflection calculations of the GFRP-Steel beam are shown Annexure-D. Experimental and calculated deflections are compared with GFRP-Steel beams in Table 4.11.

Table 4.11 Deflection comparisons calculated versus experimental of M30 and M35 GFRP-Steel beams

Beams	Calculated deflection of the M30 beam	Experimental deflection of the M30 beam	Calculated deflection of the M35 beam	Experimental deflection of the M35 beam
G1	3.853	3.871	3.650	3.659
G2	3.229	3.248	2.734	2.737
G3	2.258	2.260	2.300	2.295
G4	1.663	1.655	1.976	1.982

4.3.3. Comparison between Steel Beams and GFRP-Steel Beams on End Deflection

If the comparison is made on the basis of experimental data between the deflections then there is a considerable difference between the bars of steel and GFRP-Steel shown in Table 4.12 and 4.13.

Table 4.12 Comparison of averaged experimental deflection between M30 beams

Comparison between beams	Deflection of steel beams (mm)	Deflection of GFRP-Steel beams(mm)	Difference between deflection (mm)
S1 and G1	1.242	3.871	2.629
S2 and G2	1.264	3.248	1.984
S3 and G3	1.187	2.260	1.073
S4 and G4	1.253	1.655	0.402

Table 4.13 Comparison of averaged experimental deflection between M35 beams

Comparison between beams	Deflection of steel beams (mm)	Deflection of GFRP-Steel beams(mm)	Difference between deflection (mm)
S1 and G1	1.305	3.659	2.354
S2 and G2	1.298	2.737	1.439
S3 and G3	1.291	2.295	1.004
S4 and G4	1.346	1.982	0.636

4.4. LOAD-DEFLECTION BEHAVIOURS

The load-deflection curves of all 32-beams are plotted by the deflection at each kilo-newton of load with the help of dial gauge fitted just at mid-span of the beam while applying load. This process gives the idea of the deflection of the beam at particular load.

4.4.1. Load-Deflection Behaviours of Steel Beams

Load-deflection curves of all the steel beams are shown in Figure 4.1.

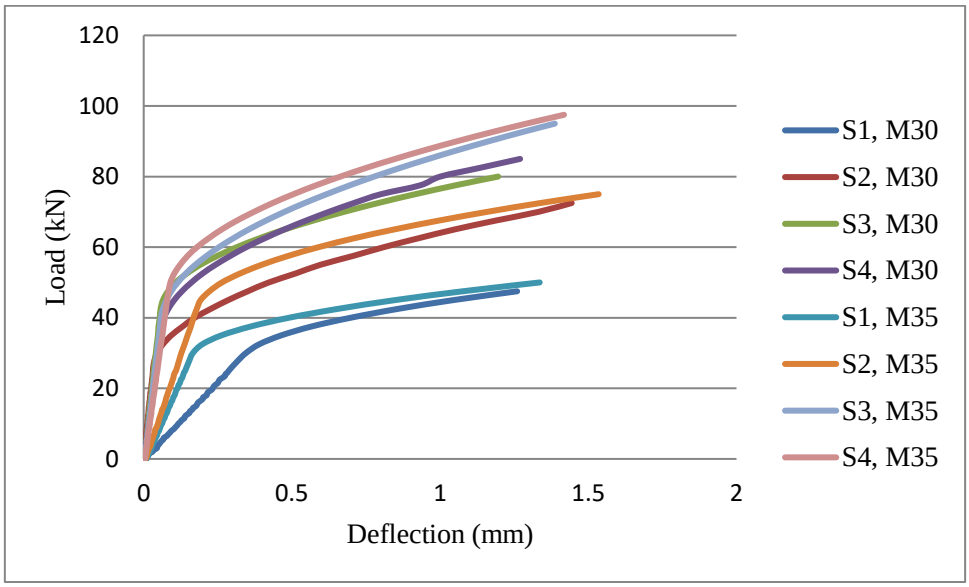

Figure 4.1 Graphs of the all steel beams of both grade M30 and M35

All of the steel beams show the same behaviour first they show the steep increase in the load with very less deflection and then at a certain point the rate of load increment starts decreasing and deflection starts to shoot up at a very high rate which will give an indication of the starting of the steel yielding. When the load is increasing steeply the load-deflection curve shows a straight line graph calling this portion of the graph as linearity period of the

graph. The load capacity in linearity period increases with increase in the reinforcement ratio and deflection in the linearity period decreases as the reinforcement ratio increase.

4.4.2. Load-Deflection Behaviour of GFRP-Steel beams

Load-deflection curves of all the GFRP-Steel beams are shown in Figure 4.2.

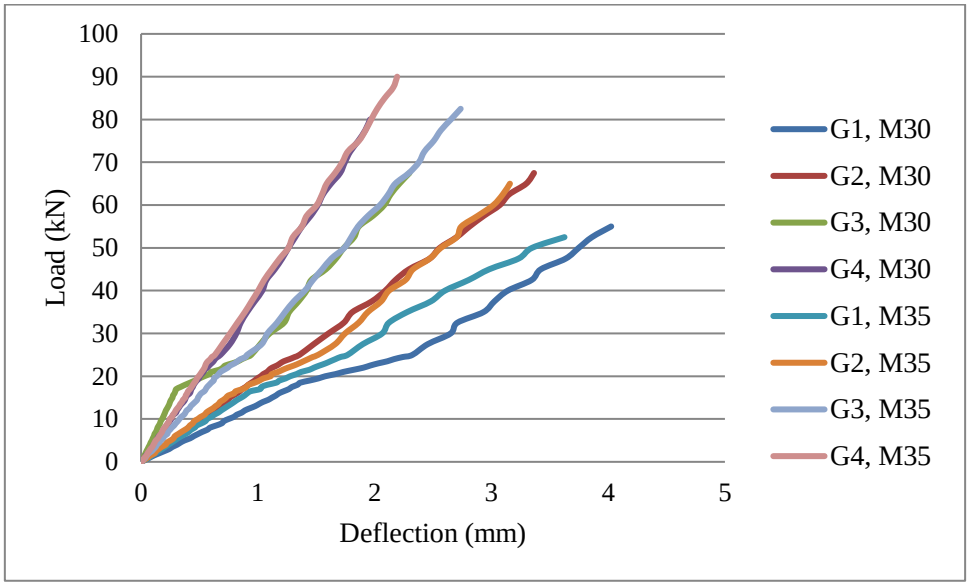

Figure 4.2 Graphs of the all GFRP-Steel beams of both grade M30 and M35

All GFRP-Steel beams nearly a linear behaviour throughout the load taking process with not much change in slope. Although some indication of the linearity period is present up to the approximate one-third or one-fourth of peak load in all beams and deflection at that time is in between 0.5 to 1.2 mm. After the linearity period, there are fluctuations in every GFRP-Steel beam i.e. no exactly straight line is seen. As the reinforcement ratio and ultimate load is increasing the deflection in beams is decreasing.

4.4.3. Comparison between Steel Beams and GFRP-Steel Beams on Load-Deflection Behaviour

The first difference between the steel and GFRP-Steel beams is deflection. Deflection of GFRP-Steel beams is far more than the steel beams. The second difference is the behaviour of failures; steel beam takes nearly half load of ultimate load-carrying capacity with very small deflection and afterwards steel beams shows large deflection with very less increment in load whereas GFRP-Steel bars show nearly linear behaviour throughout the graph. The graphs of comparison between steel and GFRP-Steel are discussed in Figure 4.3 to Figure 4.10.

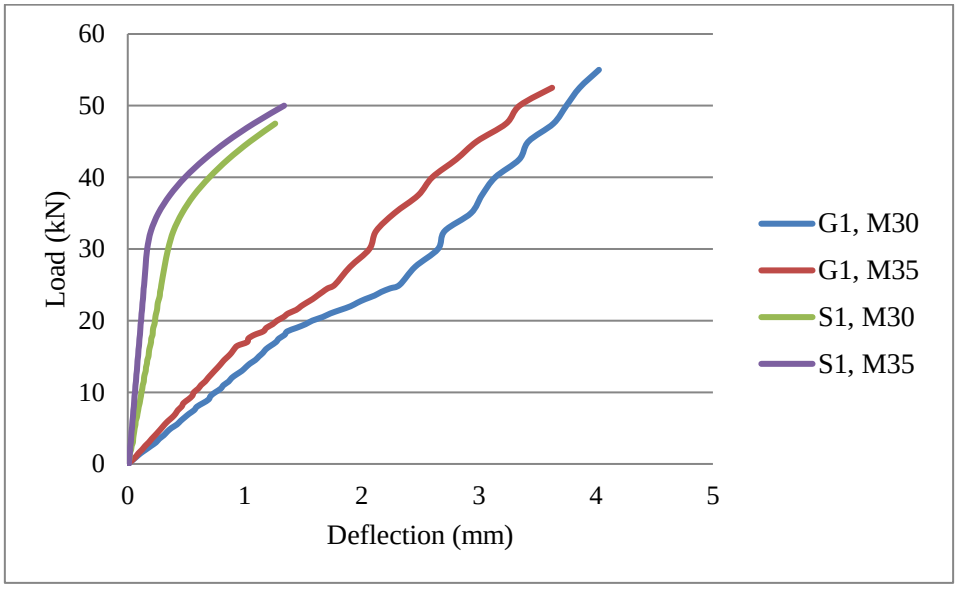

Figure 4.3 Load-deflection curve of S1 and G1 beam of grade M30 and M35.

In Figure 4.3, G1 of grade M30 shows ultimate capacity of load carrying of 55kN and mid span deflection of 4mm where S1 of grade M30 shows ultimate capacity of load carrying of 48kN and deflection of 1.5mm which is 2.6 times lesser than G1 of grade M30. G1 of grade M35 is near 52kN lesser than 3kN G1 of grade M30 and deflection of G1, M35is 3.8mm only 0.2mm lesser than G1, M30 whereas S1, M35 shows ultimate load carrying capacity of 50kN, 2kN greater than S1,M30 but lesser than G1, M35 by 2kN and deflection of S1, M35 is nearly 2.5times lesser than G1, M35.

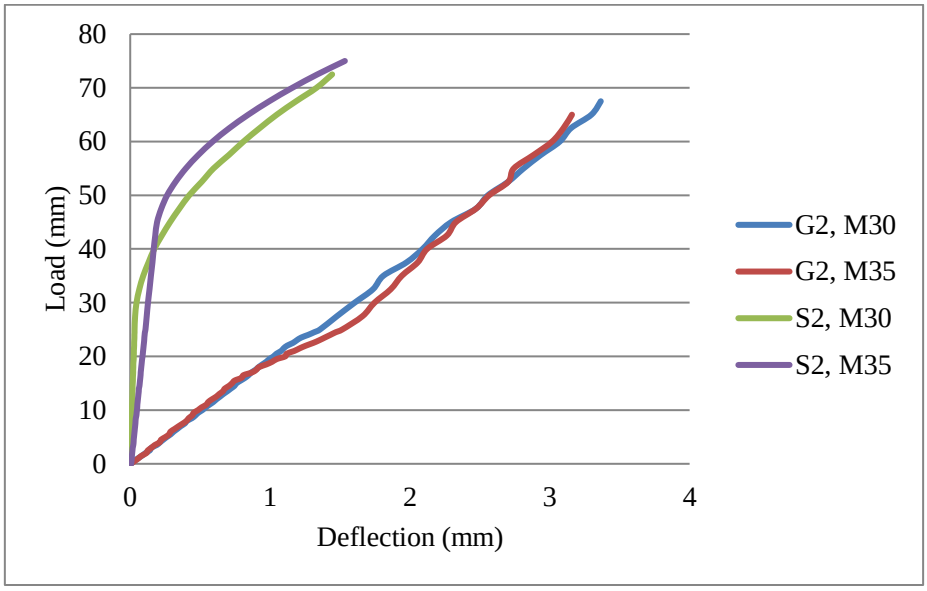

Figure 4.4 Load-deflection curve of S2 and G2 beam of grade M30 and M35.

In Figure 4.4, ultimate capacity of load carrying of G2, M30 is greater than G2, M35 by only 3kN and deflection is also 0.15mm greater in G2,M30 whereas S2, M30 is just a kilo-newton lesser than S2, M35 also deflection is 0.1mm lesser in S2, M30 than S2, M35. G2, M30

reaches near 3.2mm in the deflection and S2, M30 is just close to 1.5mm making difference of 2.13 times. In G2, M35 deflection is near 3mm and in S2, M35 it is just at 1.4mm making difference of 2.14 times.

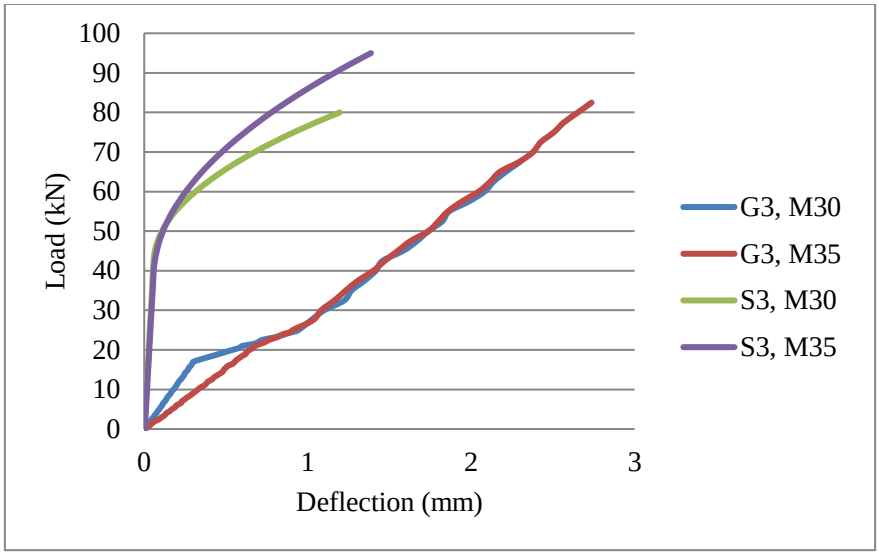

Figure 4.5 Load-deflection curve of S3 and G3 beam of grade M30 and M35.

In Figure 4.5, G3, M30 and G3, M35 ultimate load-carrying capacity differs by 9kN and in deflection the difference of 0.25mm whereas S3, M30 and S3, M35 ultimate load-carrying capacity differs by 15kN S3 and in deflection the difference of 0.2mm is noticed. The difference G3, M30 and S3, M30 deflection is of 1.25mm or 1.83 times. In G3, M35 and S3, M35 difference in deflection is 1mm or 1.66 times.

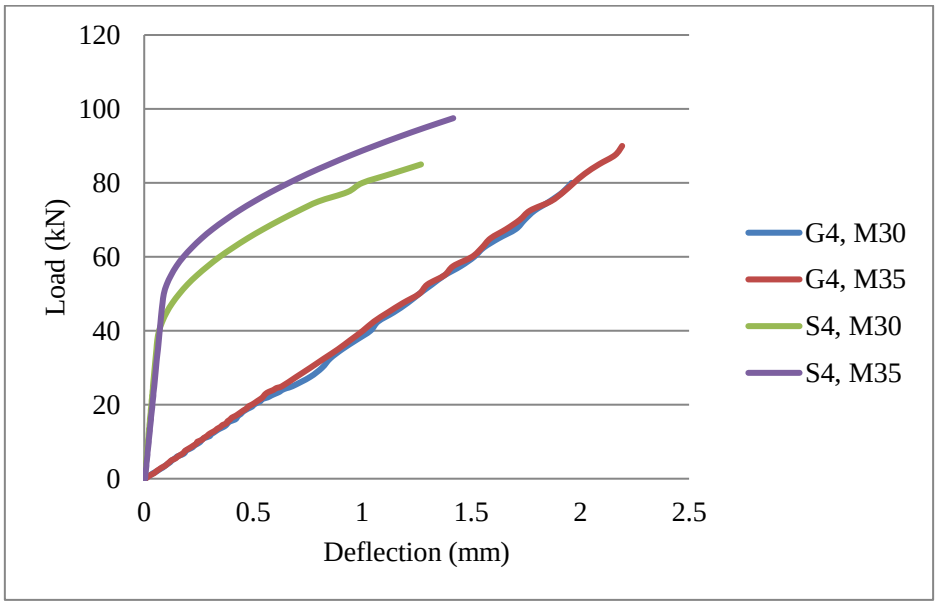

Figure 4.6 Load-deflection curve of S4 and G4 beam of grade M30 and M35.

In Figure 4.6, S4, M35 reached 98kN with deflection of 1.5mm whereas G4, M35 attained 95kn with deflection of 2.35mm making it higher 1.56 times than S4, M35 deflection.

Deflection in S4, M30 is 1.3mm and in G4, M30 is 1.8mm making 1.2 times bigger than deflection of S4, M30. Deflection difference in S4, M30 and S4, M35 is 0.2mm.

As increment is performed in the steel and GFRP-Steel beam reinforcement ratio, the distinction begins to decrease in the end deflections. The load-deflection graphs of steel and GFRP-Steel beams have huge differences in between them, steel beams load-carrying capacity increase with very less deflection in the first half of graph afterwards pattern become opposite deflection increases to fast and load increment decreases. Whereas, GFRP-Steel beams graphs is nearly linear with a little bit fluctuation. All the GFRP-steel beams have same linearity period nearly up to 20kN due to starting of de-bonding after that with deflection decreasing with increment in reinforcement ratio whereas load capacity has increased linearity period in steel with an increase in the reinforcement ratio also a little decrease in deflection is noticed with increase reinforcement in linearity period.

4.5. DUCTILITY OF BEAMS

Ductility is the material property that indicates the capacity of the material to undergo substantial plastic deformation before rupture. There are many methods to calculate the ductility but in this section, the method given by G. Appa Rao et al. (2007) is used. G. Appa Rao et al. (2007) defined ductility factor for calculating ductility which defined as the ratio of deflection at the failure to the deflection at yield or at the first crack. By this method we calculate the ductility factor of every steel and GFRP-Steel beam and then we compare with each other. More the difference between ultimate deflection and first crack deflection more will be ductility.

4.5.1. Ductility Factor Calculation of Steel Beams

As the difference between the first crack deflection and ultimate deflection is more due to the load-deflection behaviour of steel certainly the ductility will certainly be more than the GFRP beams. Ductility factor of all steel beams is shown in Table 4.25 with force value of the first crack.

Table 4.14 Values of first crack and ductility factor of steel beams

Beams	Concrete grade	First crack force (kN)		Ductility factor		Average ductility factor
		First beam	Second beam	First beam	Second beam	
S1	M30	28	20	4.058	11.654	7.856
S2		25	41	11.102	7.435	9.268
S3		37	43	20.591	21	20.795
S4		41	37	16.812	12.325	14.528
S1	M35	30	27	9.485	8.326	8.905
S2		43	32	10.153	9.526	9.839
S3		40	46	12.423	17.071	14.747
S4		49	48	17.025	11.416	14.220

4.5.2. Ductility Factor Calculation of GFRP-Steel Beams

Ductility factor of all GFRP-Steel beams in Table 4.26 with the approximate force value of the first crack.

Table 4.15 Values of first crack and ductility factor of GFRP-Steel beams

Beams	Concrete grade	First visible crack force (kN)		Ductility factor		Average ductility factor
		First beam	Second beam	First beam	Second beam	
G1	M30	18	18	3.006	2.873	2.939
G2		19	22	3.458	2.529	2.993
G3		20	22	4.249	3.006	3.627
G4		22	21	3.458	2.540	2.999
G1	M35	17	16	3.268	3.865	3.566
G2		19	20	2.533	2.848	2.690
G3		17	21	4.904	3.944	4.424
G4		21	24	3.544	3.698	3.621

4.5.3. Comparison of Ductility of Steel Beams and GFRP-Steel beams

There is much difference in the ductility of the steel beams and GFRP-Steel beams as seen steel beams are 2 to 5 times more ductile than GFRP-Steel beams which will be more cleared by Table 4.27. The reason behind more ductility of steel beams is bond strength is much

stronger than GFRP-Steel beams. Likewise, if the first crack force is seen then it is quite higher in steel beams then GFRP-Steel this is also due to the bond strength properties of steel greater than the GFRP.

Table 4.16 Comparison between ductility factor of steel beams and GFRP-Steel beams

Beams	Concrete grade	Ductility factors of steel beams	Ductility factors of GFRP-Steel beams	Difference between (1) and (2)
S1 and G1	M30	7.856	2.939	4.917
S2 and G2		9.268	2.993	6.275
S3 and G3		20.795	3.627	17.168
S4 and G4		14.528	2.999	11.529
S1 and G1	M35	8.905	3.566	5.339
S2 and G2		9.839	2.690	7.149
S3 and G3		14.747	4.424	10.323
S4 and G4		14.220	3.621	10.599

4.6. ENERGY ABSORPTION OF BEAMS

Energy absorption of beams can be calculated by the help of the load-deflection curve. The area under the load-deflection curve gives the energy absorption of the beam.

4.6.1. Energy Absorption of Steel Beams

The energy absorptions of steel beams are presented in Table 4.28.

Table 4.17 Values of energy absorption of steel beams

Beams	Concrete grade	Energy absorption (kN/mm)		Average energy absorption
		First beam	Second beam	
S1	M30	43.181	40.044	41.612
S2		43.797	79.533	61.665
S3		73.268	78.348	75.808
S4		79.893	83.527	81.710
S1	M35	49.954	54.611	52.282
S2		94.032	47.867	70.949
S3		100.125	79.882	90.003
S4		87.558	109.867	98.712

4.6.2. Energy Absorption of GFRP-Steel Beams

The energy absorptions of steel beams are presented in Table 4.29.

Table 4.18 Values of energy absorption of steel beams

Beams	Concrete grade	Energy absorption (kN/mm)		Average energy absorption
		First beam	Second beam	
G1	M30	101.365	87.486	94.425
G2		109.662	91.257	100.459
G3		78.755	69.652	74.203
G4		35.089	75.752	55.420
G1	M35	93.858	99.722	96.790
G2		52.598	94.254	73.660
G3		103.855	56.142	79.998
G4		62.353	96.912	79.633

4.6.3. Comparison of Energy Absorption of the Steel Beams and GFRP-Steel Beams

In steel, the increase in the energy absorption can be noticed with the increase of reinforcement but GFRP-Steel beams energy absorption starts decreasing with increment in the reinforcement ratio. Comparing of energy absorption of steel beam and GFRP-Steel beam is shown in Table 4.30.

Table 4.19 Comparison between energy absorption of steel beams and GFRP-Steel beams

Beams	Concrete grade	Energy absorption of steel beams	Energy absorption of GFRP-Steel beams	Difference between (1) and (2)
S1 and G1	M30	41.612	94.425	52.813
S2 and G2		61.665	100.459	38.794
S3 and G3		75.808	74.203	-1.605
S4 and G4		81.710	55.420	-26.290
S1 and G1	M35	52.282	96.790	44.508
S2 and G2		70.949	73.660	2.711
S3 and G3		90.003	79.998	-10.005
S4 and G4		98.712	79.633	-19.079

4.7. CRACK PATTERN ANALYSIS OF BEAMS

Every beam is very deeply observed for the crack patterns. Most of the beams are failed in the mixed behaviour of shear, flexure and compression. The crack pattern of every discussed with help of images in this section. In all section 4.7, S1 (1) stands for first beam of S1 and S1 (2) stands for second beam of S1 likewise this is applicable for all the beams.

4.7.1. Crack Patterns of Control Beams

4.7.1.1.Crack Patterns of S1 Beams

S1 (1) of grade M30 beam on complete failure few of the flexure cracks are generated even in the non-shear zone but at the time of ultimate collapse the shear cracks came into the dominate condition and UTM declared the ultimate failure of at 46.95kN with mix flexo-shear cracks as shown in Figure 4.7.

Figure 4.7 Cracks in S1 (1) of grade M30 beam at ultimate load 46.95kN

Figure 4.8 Cracks in S1 (1) of grade M30 beam at ultimate load 48.21kN

Figure 4.9 Cracks in S1 (1) of grade M35 beam at ultimate load 50.24kN

Figure 4.10 Cracks in S1 (2) of grade M35 beam at ultimate load 52.16kN

Both S1 (1) and S1 (2) of grade M35 beams have failed in pure flexure few of the shear cracks are seen in the both the beams but they are not the dominant cracks which caused the failure also crushing of concrete can be seen in both the beams at the upper side on time of failure. The under-reinforced beam as expected had failed in pure flexure as shown in Figure 4.9 and Figure 4.10.

4.7.1.2.Crack Patterns of S2 Beams

At the ultimate force S2 (1) of grade M30 beam as shown in Figure 4.11 shows clear failure in shear at one side while on the non-shear zone some of the flexure cracks can be seen the reason for shear failure can less shear reinforcement but shear reinforcements are already provided in more quantity than its need. Shear failure may be occurred due to less dimension of the beam or losing of the bond between the concrete and steel. S2 (1) beam also failed before it is expected so maybe there is some displacement of the reinforcement at the time of casting.

Figure 4.11 Cracks in S2 (1) of grade M30 beam at ultimate load 54.85kN

Figure 4.12 Cracks in S2 (2) of grade M30 beam at ultimate load 72.34kN

In Figure 4.12, S2 (2) beam of grade M30 fails in shear failure with some of the flexure cracks in the non-shear zone are clearly noticed. It cannot be completely called shear failure because flexure cracks are present in the beam. It may be possible that at particular point steel also starts to show de-bonding with concrete due to lesser dimensions and due to it some extra force travels to shear zone causing shear failure. No concrete compression failure is seen on the upper part of the beam.

Figure 4.13 Cracks in S2 (1) of grade M35 beam at ultimate load 78.61kN

Figure 4.14 Cracks in S2 (2) of grade M35 beam at ultimate load 58.03kN

In Figure 4.13, S2 (1) of grade M35 beam we can see same pattern of the shear failure as expected from it while S2 (2) of grade M35 beam shown in Figure 4.14 just failed badly due to failure of bond between the steel and concrete at one side crack just looks like shear at one side but a complete block of the concrete has been separated from it causing it to not achieving the force or moment capacity which is needed.

4.7.1.3.Crack Patterns of S3 Beams

Both S3 beams show nearly same behaviour which is shown by the S2 (2) beam also, first they show flexure cracks and afterwards they just abruptly fails in shear as shown in Figure 4.15 and 4.16. Beams are nearly failing at the same moment in which they are expected but not, in the same manner, maybe due to shorter dimension a/d ratio are playing a great role here.

Figure 4.15 Cracks in S3 (1) of grade M30 beam at ultimate load 79.14kN

Figure 4.16 Cracks in S3 (2) of grade M30 beam at ultimate load 80.8kN

Figure 4.17 Cracks in S3 (1) of grade M35 beam at ultimate load 95.92kN

Figure 4.18 Cracks in S3 (2) of grade M35 beam at ultimate load 84.15kN

Same type of failure behaviour is shown by earlier S3 beams of grade M30 over-reinforced beam but due to early shear cracks in the S3 (2) of grade M35 beam as shown in Figure 4.18, it just collapsed at 84kN whereas S3 (1) of grade M35 beam as shown in Figure 4.17, just gone to 95kN which means S3 (2) of grade M35 is already weak due some of the casting defects in it.

4.7.1.4.Crack Patterns of S4 Beams

In Figure 4.19, S4 (1) of grade M30 beam shows same behaviour of failure as shown by the S3 beams so in this same reasons will be applicable as before described while in S4 (2) of grade M30 as shown in Figure 4.20, beam only one side beam has failed in shear but taking nearly the same load which is taken by S4 (1) of grade M30 beam it may be due to some extra shear reinforcement has been provided in the section which hasn't failed due to the fault on making time of skeleton of the beam.

Figure 4.19 Cracks in S4 (1) of grade M30 beam at ultimate load 82.88kN

Figure 4.20 Cracks in S4 (2) of grade M30 beam at ultimate load 85.11kN

Figure 4.21 Cracks in S4 (1) of grade M35 beam at ultimate load 89.00kN

Figure 4.22 Cracks in S4 (2) of grade M35 beam at ultimate load 98.63kN

Similar behaviour is shown by the S4 (2) beam of grade M35 displayed in Figure 4.22 at the time of failure as expected but S4 (1) beam of grade M35 as shown in Figure 4.21 failed in one-sided shear which led to not completion favourable force capacity achievement of the beam.

4.7.2. Crack Patterns of GFRP-Steel Beams

4.7.2.1.Crack Patterns of G1 Beams

On the time of failure many flexure cracks can be seen in the G1 (1) of grade M30 beam but at the end very rapidly shear cracks are generated on both sides of the beam and it failed in the mix behaviour of flexo-shear failure. This must be due to the less modulus elasticity of the GFRP bar which causes de-bonding with concrete at the last stage and causes abrupt shear failure at the end. Also, the compression failure of the upper layer of concrete can be observed in Figure 4.23 of the beam.

Figure 4.23 Cracks in G1 (1) of grade M30 beam at ultimate load 56.75kN

Figure 4.24 Cracks in G1 (2) of grade M30 beam at ultimate load 52.7kN

In Figure 4.24, G1 (2) of grade M30 beam also shows the same pattern of failure just at somewhat 2kN more than the G1 (1) of grade M30 beam.

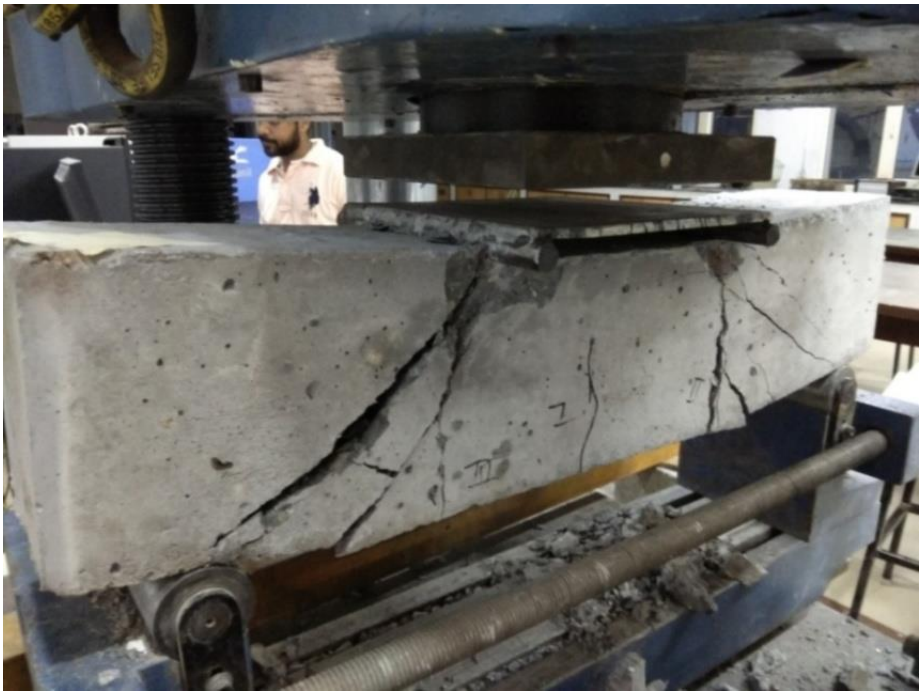

Figure 4.25 Cracks in G1 (1) of grade M35 beam at ultimate load 53.67kN

Figure 4.26 Cracks in G1 (2) of grade M35 beam at ultimate load 52.57kN

As known from the early crack pattern analysis that G1 (1) of grade M35 beam as shown in Figure 4.25 just failed in the same way, first giving many flexure cracks at centre and then it abruptly fails in the shear while G1 (2) of grade M35 beam as shown in Figure 4.26 just cracked in shear at just one end may be due to misplacement of skeleton while casting or just

any other making one end stronger than other but it failed nearly at same force at which G1 (1) of grade M35 beam failed by which above phenomenon can be explained.

4.7.2.2.Crack Patterns of G2 Beams

In both G2 beams of grade M30 show same nature of failure as expected from them. Firstly, large width flexure crack is present and then abruptly near failure, it starts to generate large shear cracks. This is the simple reason for bonding failure between GFRP bars and concrete and also a reason for the bigger deflection which is shown by the beams in Figure 4.27 and Figure 4.28.

Figure 4.27 Cracks in G2 (1) of grade M30 beam at ultimate load 67.75kN

Figure 4.28 Cracks in G2 (2) of grade M30 beam at ultimate load 63.18kN

Figure 4.29 Cracks in G2 (1) of grade M35 beam at ultimate load 49.92kN

Figure 4.30 Cracks in G2 (2) of grade M35 beam at ultimate load 66.26kN

In G2 (1) of grade M35 as shown in Figure 4.29 the same type of failure is seen as discussed in the above section at time S2 (2) of grade M35 de-bonding between the steel and concrete and steel at one side causing it to fail at the lower value than expected from it. Whereas G2 (2) of grade M35 as shown in Figure 4.30 have shown the normal failure pattern as shown by all the normal beams.

4.7.2.3.Crack Patterns of G3 Beams

Both G3 (1) and G3 (2) of grade M30 as shown in Figure 4.31 and 4.32 respectively, beams have failed as expected and same as before as in the G2 of grade M30 beams are seen and have the same reason which is elaborated before.

Figure 4.31 Cracks in G3 (1) of grade M30 beam at ultimate load 68.23kN

Figure 4.32 Cracks in G3 (2) of grade M30 beam at ultimate load 66.17kN

Figure 4.33 Cracks in G3 (1) of grade M35 beam at ultimate load 89.91kN

Figure 4.34 Cracks in G3 (2) of grade M35 beam at ultimate load 56.93kN

In Figure 4.33, G3 (1) of grade M35 beam just showed normal failure as expected from it going to force of 89kN but G3 (2) of grade M35 as shown in Figure 4.34, just again showed the defect of one side shear failure means weakness in one side of the beam due to skeleton defect or skeleton placement defect also main reinforcement also got ruptured at end of failure due to development compressive stress development in bar after the concrete splashing causing a dangerous failure falling apart of beam in 2 parts.

4.7.2.4.Crack Patterns of G4 Beams

In Figure 4.35, G4 (1) of grade M30 beam has shown the same problem as discussed before for G2 (2) of grade M35beam failing from just one side in shear but this beam also shown some shear cracks at time it reaches 50kN means certainly there is problem in the manufacturing of the beam otherwise it has shown same strength which is shown by G4 (2) beam as shown in Figure 4.36. Second G4 beam has shown the same behaviour except some of the crushing of concrete at the upper part of the beam.

Figure 4.35 Cracks in G4 (1) of grade M30 beam at ultimate load 55.77kN

Figure 4.36 Cracks in G4 (2) of grade M30 beam at ultimate load 80.2kN

Figure 4.37 Cracks in G4 (1) of grade M35 beam at ultimate load 73.86kN

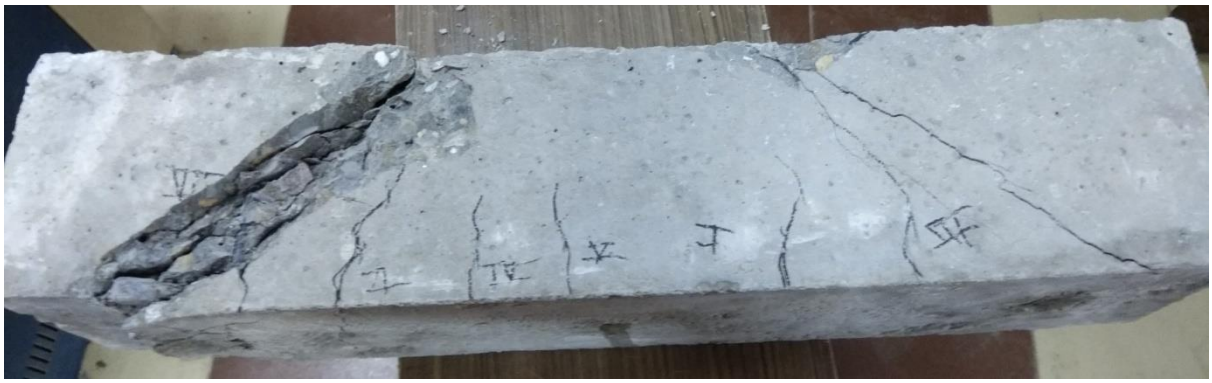

Figure 4.38 Cracks in G4 (2) of grade M35 beam at ultimate load 90.7kN

Similar behaviour of failure of G4 (1) and G4 (2) of grade M35 beams as shown in Figure 4.37 and 4.38 are seen as seen before in normal beams first many flexure cracks are seen propagating at the non-shear zone and then abrupt shear failure take place after achieving nearly calculated force.

4.7.3. Comparison of Crack Patterns of Control and GFRP-Steel Beams

3 under-reinforced steel beams failed in pure flexure behaviour and 1 showed mix behaviour of flexure and shear failure but in GFRP-Steel same reinforcement ratio beams all fails in the mixed behaviour of flexure and shear. First flexure cracks dominated in all the GFRP beams and then an abrupt failure in shear is seen at last whereas other steel beams which are doubly-reinforced has first shown small flexure cracks at a higher load than GFRP-Steel beams and then failed in shear failure happened due to the problem of the aspect ratio of beam. Flexure cracks width in the GFRP-Steel beam is much greater than steel beams if compared at a specific load.

CHAPTER-5

CONCLUSION

5.1. GENERAL

For comparing the performance difference between the steel rebars and GFRP rebars replacement of the steel rebars from the main reinforcement is done with the GFRP rebars in the casted beams in the concrete grade of M30 and M35 and afterwards two-point load is done on them to know the difference between them in the various properties like ultimate load, deflection, ductility and crack patterns. Firstly the manual calculation is done and then it is compared with the experimental results. Conclusions on all the properties are drawn and compared between are discussed below.

- The ultimate load carrying capacity is nearly achievable in both GFRP and steel with a maximum percentage error of 10.64% in GFRP-Steel beams and 12.57% in the steel beams. The maximum error in the calculated moment between the beam of steel and GFRP-Steel is nearly 28.76 % whereas in the experimental data it just decreased to 19.45%. On overall circumstances, it can be concluded that on the basis of ultimate capacity of load carrying after designing with ACI code GFRP-Steel beam can be used at the place of the steel beam whose designing is done by IS code which has the same ultimate load-carrying capacity.
- When on the basis of steel and GFRP-Steel beams are compared on the basis of deflection then the difference of maximum 2.629mm is seen in S1 beam and when the reinforcement ratio is increased it comes to a difference of 0.402mm in S4. As clearly can be seen deflection difference decrease by increasing the reinforcement ratio.
- As load-deflection curve in steel beams curve first load increases very rapidly with very less deflection in a linear manner and then achieving half the ultimate load the curve changes from linearity to different degree by which load increases very slowly and deflection increase at a very high rate that change in behaviour tells the starting of yielding of steel. On the other side, GFRP-Steel beams do not show such behaviour it just shows nearly straight line till ultimate failure. In, GFRP-Steel no specific yielding point is shown so deflection increases due to de-bonding of the GFRP rebars with concrete with an increase in force. De-bonding occurs due to low elastic modulus of the GFRP rebars.
- Ductility is calculated by taking the ratio of ultimate deflection to the deflection at first cracking point. The ductility of steel beams is greater than the GFRP-Steel. Steel

beams have 2 to 10 times more ductility than GFRP-Steel as calculated in this experiment process.

- Energy absorption of steel beams has increased with increase in reinforcement ratio whereas in GFRP-Steel beam energy absorption started to decrease with increase in reinforcement ratio. The maximum energy absorption difference is observed in S1 and G1 beam of grade M30 of 52.813kN/mm whereas the minimum is noticed in S3 and G3 beam of grade M30 of 1.605kN/mm.
- At ultimate load, few of the under-reinforced steel beams shows pure flexure failure pattern where all other beams show mixed failure condition first they show flexure cracks which are very large in GFRP-steel beams and low in the steel beams and at last all of them show abrupt shear cracks. It can because of de-bonding and small aspect ratio of beams.
- Although, flexural properties of GFRP is bit lesser than steel but in the other aspects like less weight, non-corrosive behaviour and low manufacturing cost GFRP can be used in the replacement of the conventional steel by applying some of the more safety factor restraints.

5.2. FUTURE SCOPE OF WORK

- Surface quality of the GFRP bars can be improved by adding some other resins or some mixed fibres can be used to achieve the behaviour like steel bars, so that problem of de-bonding can be reduced.
- Additional fibres or other material should be determined at which both GFRP and steel will exhibit similar properties in all aspects.
- Some extra outer wrapping will be used so that ductility and energy absorption like steel can be achieved at higher reinforcement ratio also.

ANNEXURE- A

DERIVATION OF EQUATION FOR ULTIMATE LOAD WITHOUT CONSIDERING PARTIAL SAFETY FACTORS WITH HELP OF IS-456:2000

Ultimate strain concrete ε = 0.00425 (from Graph Dawid Pawtowski and Maciej Szumigata (2015))

$$\varepsilon_y = 0.002 + \frac{f_y}{E_s}$$ (Removing 0.87 from as given IS456:2000) (1)

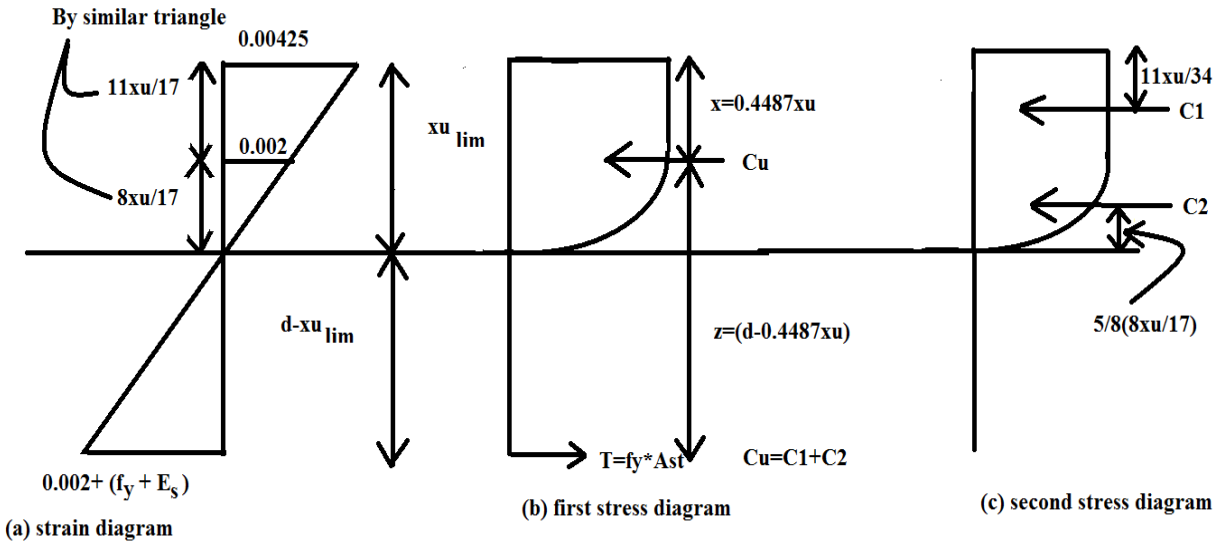

Figure-A1 New stress and strain diagram developed after removing partial safety factor

From similar triangle in strain diagram

$$\frac{0.00425}{x_{u\,lim}} = \frac{\frac{f_y}{E_s}+0.002}{d-x_{u\,lim}} \quad => \quad \frac{x_{u\,lim}}{d} = \frac{850}{1250+f_y}$$

Taking f_y= 560 N/mm^2

$$=> \frac{x_{u\,lim}}{d} = 0.469$$ (2)

Now for compressive force (second stress diagram)

$$C_u = f_{ck}\left(\frac{11}{17}x_u b\right) + \frac{2}{3}\left(f_{ck}\frac{8}{17}x_u\right)b$$

$$=> C_u = 0.96 f_{ck} x_u b$$ (3)

For $\bar{x}$ (second stress diagram)

$$C_u\bar{x} = C_1 \times \frac{11}{34}x_u + C_2\left(x_u - \frac{5x_u}{17}\right)$$

$$=> \bar{x} = 0.4487x_u \quad (4)$$

For Neutral axis,

$$0.96f_{ck}bx_u = f_yA_{st}$$

$$=> x_u = \frac{f_yA_{st}}{0.96f_{ck}b} \quad , \text{if } x_u \leq x_{u\,lim} \quad (5)$$

For Moment of resistance,

From the compression side,

$$M_u = C_u \times z$$

$$M_u = 0.96f_{ck}bx_u(d - 0.4487x_u) \quad (6)$$

From tension side,

$$M_u = T \times z$$

$$M_u = f_yA_{st}(d - 0.4487x_u) \quad (7)$$

If $x_u = x_{u\,lim}$

$$M_{u\,lim} = f_{ck}bd^2\left\{0.96\frac{x_{u\,lim}}{d}(1 - 0.4487\frac{x_{u\,lim}}{d}\right\}$$

or

$$M_{u\,lm} = f_yA_{st}(d - 0.4487x_{u\,lim}) \quad (8)$$

If $x_u < x_{u\,lim}$

$$M_u = f_yA_{st}(d - 0.4487x_u) \quad (9)$$

or

$$M_u = f_yA_{st}(d - 0.4487\frac{f_yA_{st}}{0.96f_{ck}b}) \quad (10)$$

ANNEXURE- B

CALCULATION OF MOMENT OF GFRP-STEEL G2 BEAM ACCORDING TO ACI440.1R-06, DESIGN OF SHEAR REINFORCEMENT ACCORDING TO IS-456:2000 AND DESIGN OF S2 STEEL BEAM ACCORDING TO CALCULATED MOMENT GFRP-STEEL BEAM WITH HELP OF IS-456:2000

Taking G2 beam i.e. 3 bars of 10mm GFRP at the bottom and 2 bars of 8mm steel at the upper part of the beam of grade M30

Beam length (l) = 700mm

Beam breadth (b) = 150mm

Beam depth (h) = 150mm

Effective depth of beam (d) = 150 – 28 = 122mm

GFRP bars number = 3

GFRP bar diameter (d_b) = 10mm

Area of GFRP bars (A_f) = $\frac{(3\times\pi\times10^2)}{4} = 235.619\text{mm}^2$

GFRP reinforcement ratio (ρ_f) = $\frac{A_f}{bd} = \frac{235.619}{150\times150} = 0.012875$

Strength in compression of concrete ($f_c^{'}$) = 30.57 MPa

Strength in tension of GFRP bars (f^{*}_{fu}) = 980 MPa

Design rupture strength (f_{fu}) = $C_E \times f^*_{fu} = 0.8 \times 980 = 784\text{MPa}$ (C_E= 0.8, concrete not exposed earth weather)

Elastic modulus of GFRP (E_f) = 60000 MPa

Ultimate strain in concrete (ε_{cu}) = 0.0035 (recommended in IS456:2000)

Factor β_1 = 0.8321 (the factor is taken as 0.85 for compressive strength fc′ up to and including 28 MPa, for quality over 28 MPa, this factor is diminished consistently at a rate of 0.05 per 7 MPa of solidarity more than 28 MPa, yet isn't taken under 0.65)

GFRP reinforcement ratio producing balanced strain condition (ρ_{fb}) = $0.85\frac{f'_c}{f_{fu}}\beta_1\frac{E_f\varepsilon_{cu}}{E_f\varepsilon_{cu}+f_{fu}} = 0.00582$

$\rho_f > \rho_{fb}$ (under-reinforced)

Stress in GFRP reinforcement in tension (f_f) = $\sqrt{A+B}-C$

Where, A = $\frac{(E_f\varepsilon_{cu})^2}{4} = 11025$, B = $\frac{0.85\beta_1 f'_c}{\rho_f}E_f\varepsilon_{cu} = 352654.6$ and C=$0.5E_f\varepsilon_{cu} = 105$

So, $f_f = \sqrt{A+B} - C = \sqrt{11025 + 352654.6} - 105 = 498.058\text{MPa}$

Nominal moment capacity $M_n = \rho_f f_f \left(1 - 0.59\frac{\rho_f f_f}{f_c'}\right) bd^2 = 12545031\text{Nmm or } 12.545\text{ kNm}$

Maximum shear force according to nominal moment (V_u) = $\frac{(Mn \times 3)}{l'}$ = 62725.15N or 62.725kN

Where, l' = testing length of beam section = 600mm

$$\tau_v = \frac{V_u}{b \times d} = \frac{62725.15}{150 \times 122} = 3.427\text{N/mm}^2$$

$$\frac{100A_f}{b \times d} = \frac{100 \times 235.619}{150 \times 122} = 1.287\text{N/mm}^2$$

τ_c= 0.454N/mm^2 (from IS-456:2000)

Spacing provided if steel provided is 8mm 2 legged stirrups A_{sv}= 100.530mm^2

Minimum of $\frac{0.87A_{sv}f_y}{(\tau_v - \tau_c) \times b}, \frac{2.175A_{sv}f_y}{b}$, 0.75*d and 300mm, where f_y= yielding strength of steel (Fe500)

That is 91.5mm to be more protective stirrups are provided at 60 mm c/c distance.

Now for designing steel beam for the same moment as of GFRP beam of the same dimension.

Taking, Yielding stress f_y= 560 N/mm^2, lower cover d'= 15mm, compressive stress of concrete f_{ck}= 31.52 N/mm^2 and effective depth (d) = 121mm (150 - 15 - 8(stirrups) - 6(assuming 12mm main reinforcement)

$$\frac{x_{u,max}}{d} = \frac{700}{1100 + (0.87f_y)} = 0.441 \text{ or } x_{u,max} = 53.364\text{mm}$$

Given moment, M = 12545031Nmm or 12.54503 kNm

Moment of resistance, $M_{u,\,lim} = 0.36\left(\frac{x_{u,max}}{d}\right)\left(1 - 0.416\frac{x_{u,max}}{d}\right) f_{ck} bd^2 = 8974090\text{Nmm}$

Moment of resistance, $M_{u,\,lim}$ < Given moment M. So, the beam will be designed as an over-reinforced beam.

Limiting the reinforcement ratio, $\rho_{t,lim} = \frac{0.414f_{ck}\left(\frac{x_{u,max}}{d}\right)}{f_y}$ =0.103

Limiting tensile reinforcement, $A_{st,lim} = \rho_{t,lim} bd = 186.527\text{mm}^2$

Extra tensile reinforcement required, $A_{st2} = \frac{M - M_{u,lim}}{0.87f_y(d - d')}$ = 69.146mm^2

Total tensile reinforcement = $A_{st,lim} + A_{st,2} = 186.527 + 69.146 = 255.673mm^2 < max.A_{st} = 0.04bh = 900mm^2$

Strain considered in compression steel in this beam, $\varepsilon_{sc} = 0.0035\frac{(d'-x_{u,max})}{x_{u,max}}$ = 0.0025

Stress considered in compression steel in this beam, f_{sc} = 402.201N/mm^2 (from IS-456:2000)

Area of compression steel, $A_{sc} = \frac{M-M_{u,lim}}{(f_{sc}-(0.446f_{ck}))(d-d')}$ =86.793mm^2

From all above, numerical taking 2 bars of 12mm as tension steel (A_{st}=226.194mm^2) and 2 bars of 8mm (A_{sc}=100.530mm^2) in compression steel and again calculating the moment of resistance for given steel.

Tensile force in steel, $T_u = 0.87f_yA_{st} = 110202N$

Assuming neutral axis x_u at 42.5mm for equalizing compression and tension force

$3x_u/7$ = 18.214mm > d', hence OK

Strain considered in compression steel in this beam, $\varepsilon_{cu} = 0.0035\frac{(d'-x_u)}{x_u}$ = 0.0022

Stress considered in compression steel in this beam, f_{sc} = 391.500N/mm^2 (from IS-456:2000)

Compression force due to concrete, $C_{cu} = 0.36f_{ck}bx_u = 72338.4N$

Compression force due to steel, $C_{su} = (f_{sc}A_{sc}) - (0.446f_{ck}A_{sc}) = 37944.61N$

Total compressive force, $C_u = C_{cu} + C_{su}$=110283N (nearly equal to C_u)

Moment of resistance for beam, $M_u = C_{cu}(d - 0.416x_u) + C_{su}(d - d') = 11496132Nmm$ or $11.4961kNm$

Maximum shear force according to nominal moment (V_u) = $\frac{(Mn\times3)}{l'}$ = 62725.51N or 62.725kN

Where, l' = testing length of beam section = 600mm

$$\tau_v = \frac{V_u}{b \times d} = \frac{55414.81}{150 \times 121} = 3.455/mm^2$$

$$\frac{100A_f}{b \times d} = \frac{100 \times 235.619}{150 \times 121} = 1.246N/mm^2$$

τ_c= 0.454 N/mm^2 (from IS-456:2000)

Spacing provided if steel provided is 8mm 2 legged stirrups A_{sv}= 100.530mm^2

Minimum of $\frac{0.87A_{sv}f_y}{(\tau_v-\tau_c)\times b}, \frac{2.175A_{sv}f_y}{b}$, 0.75*d and 300mm, where f_y= yielding strength of steel (Fe500)

That is 90.75mm to be more protective stirrups are provided at 60 mm c/c distance.

ANNEXURE- C

CALCULATION OF MOMENT OF GFRP-STEEL G1 BEAM ACCORDING TO ACI440.1R-06 AND DESIGN OF S1 STEEL BEAM ACCORDING TO CALCULATED MOMENT GFRP-STEEL BEAM WITH HELP OF NEWLY DERIVED FORMULA FROM ANNEXURE-A

Taking G2 to beam i.e. 3 bars of 8mm GFRP at the bottom and 2 bars of 8mm steel at the upper part of the beam

Beam length (l) = 700mm

Beam breadth (b) = 150mm

Beam depth (h) = 150mm

Effective depth of beam (d) = 150 – 27 = 123mm

GFRP bars number = 3

GFRP bars diameter (d_b) = 8mm

Area of GFRP bars (A_f) = $\frac{(3\times\pi\times8^2)}{4}$ = 150.796mm^2

GFRP reinforcement ratio (ρ_f) = $\frac{A_f}{bd} = \frac{235.619}{150\times150}$ = 0.00817

Strength in compression of concrete ($f_c^{'}$) = 30.57 MPa

Strength in tension of GFRP bars (f^{*}_{fu}) = 1080 MPa

Design rupture strength (f_{fu}) = $C_E \times f^*_{fu} = 0.8 \times 980 = 864$MPa ($C_E$= 0.8, concrete not exposed earth weather)

Elastic modulus of GFRP (E_f) = 60000 MPa

Ultimate strain in concrete (ε_{cu}) = 0.0035 (recommended in IS456:2000)

Factor β_1 = 0.832 (the factor is taken as 0.85 for compressive strength fc′ up to and including 28 MPa, for quality over 28 MPa, this factor is diminished consistently at a rate of 0.05 per 7 MPa of solidarity more than 28 MPa, yet isn't taken under 0.65)

GFRP reinforcement ratio producing balanced strain condition (ρ_{fb}) = $0.85\frac{f'_c}{f_{fu}}\beta_1\frac{E_f\varepsilon_{cu}}{E_f\varepsilon_{cu}+f_{fu}} =$ 0.00489

$\rho_f > \rho_{fb}$ (under-reinforced)

Stress in GFRP reinforcement in tension (f_f) = $\sqrt{A+B} - C$

Where, A = $\frac{(E_f\varepsilon_{cu})^2}{4} = 11025$, B = $\frac{0.85\beta_1 f'_c}{\rho_f}E_f\varepsilon_{cu} = 555539.3$ and C=$0.5E_f\varepsilon_{cu} = 105$

So, $f_f = \sqrt{A + B} - C = \sqrt{11025 + 352654.6} - 105 = 647.704$MPa

Nominal moment capacity $M_n = \rho_f f_f \left(1 - 0.59 \frac{\rho_f f_f}{f_c'}\right) bd^2 = 10786151$Nmm or 10.786 kNm

Now for designing steel beam for the same moment as of GFRP beam of the same dimension.

Taking, Yielding stress f_y= 560 N/mm^2, lower cover d$'$= 15mm, compressive stress of concrete f_{ck}= 31.52 N/mm^2 and effective depth (d) = 123mm (150 - 15 - 8(stirrups) - 4(assuming 8mm main reinforcement)

Moment of resistance of beam according to new formula $M_{u,\ lim} = f_{ck} bd^2 \left\{0.96 \frac{x_{u\ lim}}{d} (1 - 0.4487 \frac{x_{u\ lim}}{d}\right\}$ = 24291794Nmm or 24.29kNm

So, the beam is an under-reinforced beam. Now, taking a random beam of lower reinforcement of 3 bars of 8mm of steel and upper 2 supporting bars of 8mm and checking it for under-reinforced section by the conventional formula.

$\frac{x_u}{d} = \frac{0.87 f_y A_{st}}{0.36\, f_{ck} bd}$ = 0.35 making it an under reinforced beam as per IS456:2000

Now, using the above-derived formula to find the moment of resistance of the beam

$M_u = f_y A_{st} \left(d - 0.4487 \left(\frac{f_y A_{st}}{0.96 f_{ck} b}\right)\right.$ = 9646172Nmm or 9.646kNm

Annexure- D

CALCULATION OF DEFLECTION OF GFRP-STEEL G1 BEAM ACCORDING TO ACI440.1R-06 AND STEEL BEAM S1 WITH COMBINATION OF BOTH ACI AND INDIAN STANDARD

Taking, GFRP-Steel beam of 3 bars of 8mm of GFRP in the lower part and 2 bars of 8mm of steel in the upper part of grade M 30

Experimental ultimate moment, M_a = 10.94kNm

Gross moment of Inertia, $I_g = \frac{bh^3}{12} = \frac{150\times150^3}{12} = 42187500\text{mm}^4$

Cracked section properties and cracking moment

$f_r = 0.62\sqrt{f_c'} = 0.62\sqrt{30.57} = 3.427\text{MPa}$

$M_{cr} = \frac{2f_rI_g}{h} = \frac{2\times3.427\times42187500}{150} = 1928244\text{Nmm or } 1.928\text{kNm}$

$I_{cr} = \frac{bd^3}{3}k^3 + n_fA_fd^2(1-k)^2$

Where, $n_f = \frac{E_f}{E_c} = \frac{E_f}{4750\sqrt{f_c'}} = \frac{60000}{26262.818} = 2.284$

$k = \sqrt{2\rho_fn_f + (\rho_fn_f)^2} - \rho_fn_f = 0.1737$

So, $I_{cr} = \frac{150\times123^3}{3}(0.1737)^3 + 2.284\times150.796\times(123)^2\times(1-0.1737)^2 = 4045342.74\text{mm}^4$

Modification factor, $\beta_d = \frac{1}{5}\left[\frac{\rho_f}{\rho_{fb}}\right] = \frac{1}{5}\left[\frac{0.008173}{0.004893}\right] = 0.334$

Effective moment of Inertia, $I_e = (\frac{M_{cr}}{M_a})^3\frac{I_g}{7} + 0.84\left[1-(\frac{M_{cr}}{M_a})^3\right]I_{cr} = 4145438\text{mm}^4$

Ultimate deflection,

$\Delta_{max} = \frac{Pa}{24E_cI_{eff}}(3L^2-4a^2) = 3.852\text{mm}$

Now, taking steel beam of 3 bars of 8mm of steel in the lower part and 2 bars of 8mm of steel in the upper part

Elastic modulus of steel E_s=200000N/mm^2

Elastic modulus of concrete E_c=$5000\sqrt{f_{ck}}$=28071.337N/mm^2

Modular ratio m=$\frac{E_s}{E_c} = \frac{200000}{28071.337} = 7.124$

f_{cr}=$0.7\sqrt{f_{ck}}$=3.929N/mm^2

Transformed section,

$$\frac{1}{2}bx^2 = mA_{st}(d-x) = \frac{1}{2} \times 150 \times x^2 = 7.124 \times 150.796 \times (123-x)$$

x_1=35.420mm (taken)

x_2=-49.7452mm (rejected)

Lever arm (z) = d – (x/3) = 123 – (35.420/3) = 111.193mm

Rupturing moment of inertia, $I_r = \frac{bx^3}{3} + m\,A_{st}\,(d - x)^2$ = 10462619mm^4

Gross moment of inertia, $I_{gr} = \frac{bh^3}{12} = \frac{150 \times 150^3}{12}$ =42187500mm^4

Rupturing moment, $Mr = \frac{I_{gr}}{y_t} f_r$ =2210618N or 2.210kNm

Where y_t= line which divides the area of section into two parts = 75mm

Effective moment of inertia, $I_{eff} = \frac{I_r}{1.2 - \left(\frac{M_r}{M_u}\right)\left(\frac{z}{d}\right)\left(1 - \frac{x}{d}\right)}$ =10741599mm^4

Taking the maximum of I_r and I_{eff}, the ultimate deflection should be found

$$\Delta_{max} = \frac{Pa}{24E_c(\text{maximum of}(I_{eff} \text{or } I_r))}(3L^2 - 4a^2) = 1.398\text{mm}$$

REFERENCES

ACI Committee 440,1R-06, Guide for the design and construction of concrete reinforced with FRP bars, Flangminton Hills (MI): American Concrete Institute;2006,44pp.

ACI Committee440, R-96, State-of-the-Art Report on Fibre Reinforced Plastic (FRP) Reinforcement for Concrete Structures, American Concrete Institute;1996, 68pp.

Benmokrane B., Chaallal O.,& Masmoudi R.,(1995), Glass fibre reinforced plastic (GFRP) rebars foe concrete structures, Construction and Building Materials,9,353-364.

Caratelli A., Meda A., Rinaldi Z., Spagnuolo S.,& Maddaluno G.,(2017), Optimization of GFRP reinforcement in precast segments for metro tunnel lining, Composite Structures,181,336-346.

Faza, S. S.,& GangaRao V.,(1992), Pre-and post-cracking deflection behaviour of concrete beams reinforced with fibre-reinforced plastic rebars, In Proceedings of the First International Conference on Advanced Composite Materials in Bridges and Structures, (ACMBS-I), 129-137.

G. Appa Rao, I. Vijayanand & R. Eligehausen,(2017),Studies on the ductility of RC beams in flexure and size effect, Materials and Structures 41 (4), 759-771

Gu X., Yu B.,& Wu M.,(2016), Experimental study of bond performance and mechanical response of GFRP reinforced concrete, Construction and building material, 114,407-415.

Holly I., Bilcik J., Kesel O.,& Gazovicova N.,(2016), Bond of GFRP Reinforcement with concrete, Key Engineering Materials,691,356-365.

Indian Standard CodeIS456:2000, Plain and reinforced concrete - code of practice (fourth revision), Bureau of Indian Standards, Manak Bhavan, 9 Bahadur Shah Zafar Marg, New Delhi 110002.

Issa M. S., Metwally I.M.,& Elzeiny S.M.,(2011). Influence of fibres on flexural behaviour and ductility of beams reinforced with GFRP rebars, Engineering Structures,33,1754-1763.

Jabbar S.A.A., &Farid S.B.H.,(2018), Replacement of steel rebars by GFRP in concrete structures, Karbal International Journal of Modern Science,4,216-277.

Jarek B.,& Kubik A.,(2015), The examination of the Glass Fiber Reinforced Polymer composite rods in terms of the application of concrete reinforcement, Procedia Engineering 108,394-401.

Kaszubska M., Kotynia R.,& Barros J.A.O.,(2017), Influence of longitudinal GFRP reinforcement ratio on the shear capacity of concrete beams without stirrups, Journal of Stuctural engineering, 193,361-368

Maksikov S., Bashkova Ju.,& Maksimova A.,(2017), Modernization of Technology and Equipment for Glass Fiber Reinforced Plastic Rebar Production, Procedia Engineering,206,(2017),1337-1341.

Sheikh S.A.,& Kharal Z,(2018). Replacement of steel with GFRP for sustainable reinforced concrete. Construction and Building Materials,160,767-774.

Toutanji H.A,& Saafi M., (2000)Flexural behaviour of concrete beams reinforced with glass fibre- reinforced polymer (GFRP) bars, ACI structure Journal,97,712-719.

Vijay P,& Ganga Rao V.,(2001), Bending behaviour and deformability of glass fibre reinforced polymer reinforced concrete members, ACI structure Journal,98(6),834-842.

Yang W.-r., He X.-j.,& Dai L., (2017), Damage behaviour beams reinforced with GFRP bars, Composite structure, 161,173-186.